N° d'ordre :
N° de série :

PEOPLE'S DEMOCRATIC REPUBLIC OF ALGERIA
Ministry of Higher Education and Scientific Research

UNIVERSITY OF ECHAHID HAMMA LAKHDAR - EL OUED

FACULTY OF EXACT SCIENCES
Physics departement

Presented By:
Toufik Nefouci

End of study memory
Presented for the Diploma of ACADEMIC MASTER

Speciality : Physique
Option : Physique Appliquée Rayonnement Energétique

Theme

Spectroscopic characterization of El-oued sand dunes

Sustained on ....-June-2019

From the jury:

Mr. REHOUMA Ferhat	Professor	President
Ms. LARGOT Hanane	MAA	Reporter
Ms. MEFTAH Nassima	MBA	Supervisor

Academic year 2018 - 2019

ACKNOWLEDGEMENT

I would first like to thank my thesis Supervisor Ms. MEFTAH Nassima at Elchahid Hamma lakhdar university of El-Oued. The door to Prof. Meftah office was always open whenever I ran into a trouble spot or had a question about my research or writing. She consistently allowed this paper to be my own work, but steered me in the right the direction whenever she thought I needed it.

DEDICATION

For everyone through whose memories I live ....

Table of contents

List of tables

List of figures

General introduction

General introduction

The main motive that triggered many ideas of sand examination, is the abundance of huge amounts of sand in earth's crust, this sand is chiefly composed of quartz and other minerals, such as sand rocks, igneous rocks and Sedimentary rocks. [1] Many of these minerals are tightly related to numerous human activities, and some of their properties only came to our knowledge after studies conducted in research centers and international universities laboratories.

The results found by researchers in countries like Libya, Egypt and Tunisia have shown the presence of mutual properties among earth's crust minerals. [1] those properties are of a significant correspondence to the geographical location.

Quartz has a wide range of applications, and is considered a corner stone of many industries, for instance, building materials, thermal rocks, anti-humidity rocks and clean energy equipment. The marked quality transformation in building materials in both Egypt and Tunisia was essentially due to the studies on natural resources (generally) and quartz (specifically) utilization. Quartz is also a crucial component in electronics industry.

Silica sand is mostly comprised of silicon dioxide (SiO_2) along with small amounts of impurities and other minerals oxides, also is it covers vast areas of earth's surface. [1] The deserts around the world possess enormous amounts of minerals and natural treasures, dunes in south of Algeria has been the focus of many geological studies where only the creation and evolution of sand mattered.

Previous studies that aimed to identify sand in the south of Algeria , showed the existence of a high quartz (SiO_2) content percentage. These results were so encouraging to conduct other studies in various regions in the south of Algeria. The study of sand minerals chemical and physical properties in Algeria is very important due to its potential applications in many industries, for instance, building materials, glass making, energetics and medicine.

For the sand in Algeria to be used in future application, it has to be fully identified. This thesis is one of the first attempts to study El-Oued's sand. this study was divided into three chapters as follows:

The first chapter is concerned with the general notions of sand, and in it we discussed the definition of sand, and also presented some of its chemical and physical properties, As well as its importance to our modern industry.

The second chapter was dedicated to explain the samples gathering, the basics of the experimental methods and instruments used in the examination of sand samples. The methods covered in this chapter are X-Ray diffraction and FTIR (Fourier-transform infrared spectroscopy).

The third chapter was for the presentation and discussion the results of both FTIR and the XRD analysis.

Finally, this thesis was ended with a conclusion in which summarized the results and opened a new research door.

Chapter I

General notions on sand

I-1-Introduction

For the sake of a better understanding the interest of sand this chapter will discuss the definition of sand, and also present its chemical and physical properties, As well as its importance to our modern industry.

I-2-Sand definition:

Sand refers to solid inorganic particles that are derived from the weathering of rocks. In geology, sand is defined as mineral particles with diameters between 62.5 and 2000 µm [1].

It is conventional too to think of sand as something that is broken down from a larger mass of bedrock. However, from the viewpoint of sand being particles of a given size or, dune-forming material in general, this perspective is somewhat parochial. Snow forms dunes, yet is crystallized in the air from water vapor; Titan's sand may start in a similar way, perhaps agglutinated somehow on the surface. So material can grow into sand, not just be broken down into it [2].

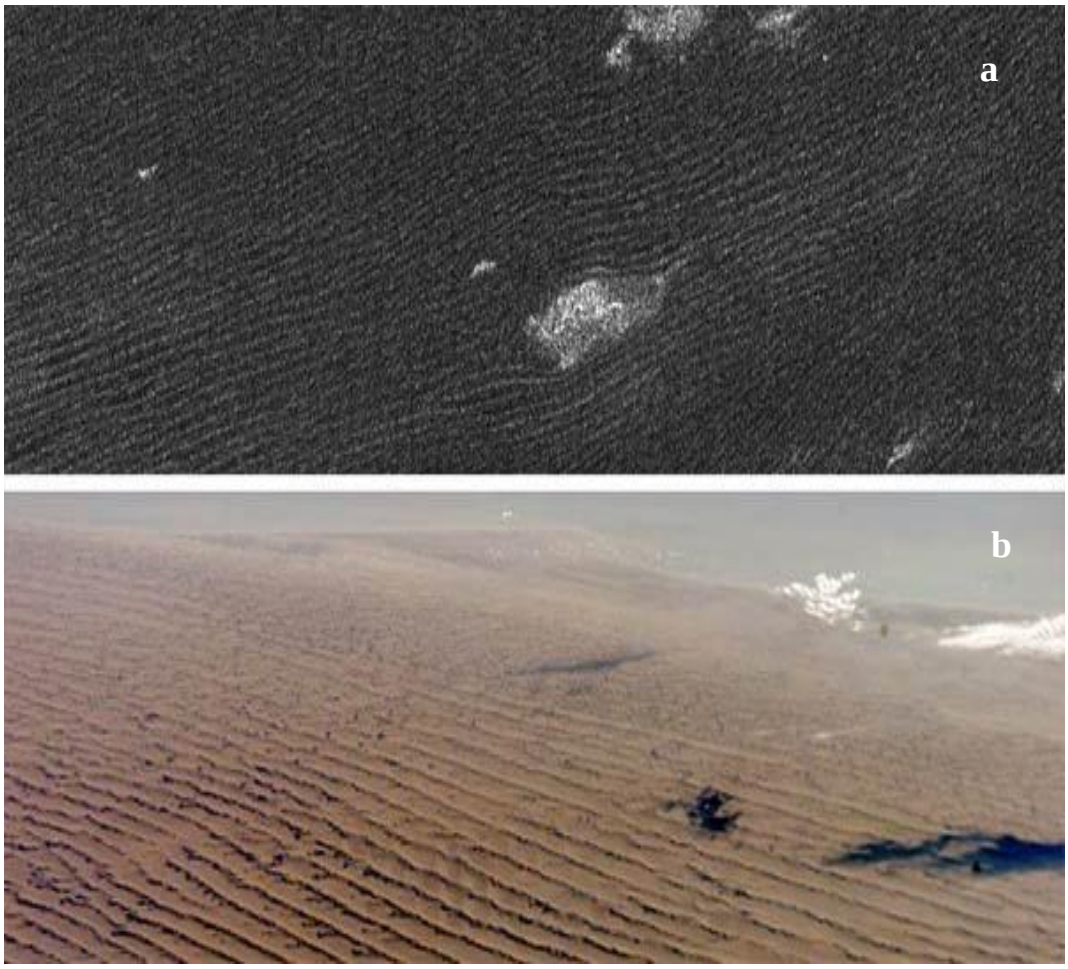

Figure I.1: Dunes on Titan seen in Cassini's radar (**a**) that are similar to Namibian sand dunes on Earth[3] (**b**).

I.3 Global Distribution of Sand Seas:

The location of the world's major active sand seas is shown in **Figure I.2**. Many of these sand seas have large areas of stabilized dunes on their margins. [5]

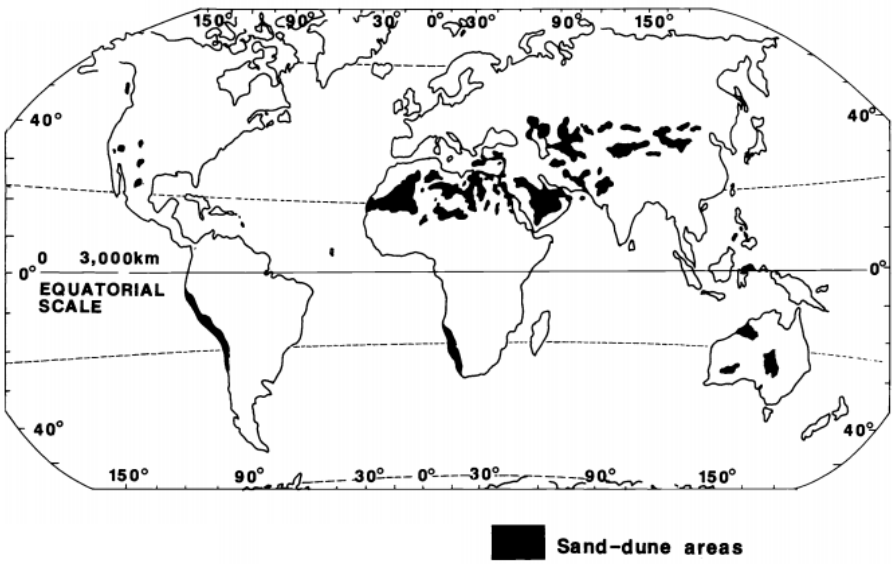

Figure I.2: Global Distribution of Sand Seas[5].

I -4-The chemical and physical properties of sand:

I -4-1- The chemical composition of sand:

Sand is mainly comprised of Quartz (SiO_2), Calcium carbonate ($CaCO_3$), Gypsum ($CaSO_4$, $2H_2O$), small amounts of impurities and heavy metals, Iron (III) Oxide (Fe_2O_3) and Aluminum oxide (Al_2O_3). The table below presents chemical compositions of sand, and the mass percentage of each compound in given samples taken from various regions around the world **(table I.1)**. [1]

Table I.1: The Chemical analysis of sand samples taken from various regions around the world[1] [23]

Oxides	Mass Percentage (%)					
Region	**The Grand Erg (Algeria)**	**Thar Desert (India)**	**Arabian Peninsula.**	**Australia**	**Vizcaíno Desert, Mexico**	**El-Oued Region (Algeria)**
SiO_2	74.61	80.37	83.42	88.37	71.38	97.63
Al_2O_3	1.35	5.53	5.12	6.46	14.24	0.327
Fe_2O_3	0.86	2.10	0.64	3.09	1.92	0.042
CaO	17.3	4.60	4.06	0.15	4.74	0.56
Na_2O		1.20		0.11	3.52	0.54
MgO	0.29	0.97	2.4	0.22	0.94	0.61

I -4-2- Sand grains:

I-4-2-1-Sand grains sizes:

According to the geological categorization, a sand grain have between 62.5 and 2,000 µm diameter, which means its smaller than gavel and larger than silt **(**table I.2**)** [2]

Table I.2: Different particles sizes and names [1]

Name	Grain diameter
Gravel	2—64 mm
Granule	2—4 mm
Sand	1/16 — 2 mm
Silt	1/256—1/16 mm
Clay	<1/256 mm

I-4-2-2- Sand Grains Morphology:

Once sand grains were observed by microscopes shape related terms like spherical, cylindrical or sheet-like came into usage. However, these terms needed to be quantified. Haakon Wadell (1935) [6] came up with a simple method based on the shape and roundness of sand grains determined through two-dimensional photographs taken by microscopes. Hakon wadell defined roundness as the ratio of the average radius of curvature circles inscribed within corners on the grain to the radius of the maximum inscribed circle within the entire grain. And shape as the ratio of the cross-sectional area of the grain to the smallest circumscribed circle. This results a maximum value for both shape and roundness equals to 1. circumscribed circle. This results a maximum value for both shape and roundness equals to 1. [7]

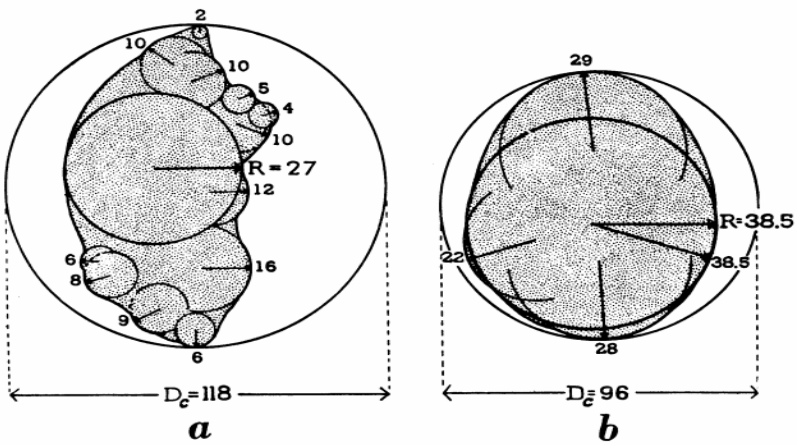

Figure I.3: A drawing shows the necessary measurements to calculate both the shape and roundness ratios (the dimensions are given in millimetres) [6] **.**

The chart below (**Figure I.4)** is used to classify sand grains according to roundness and shape.

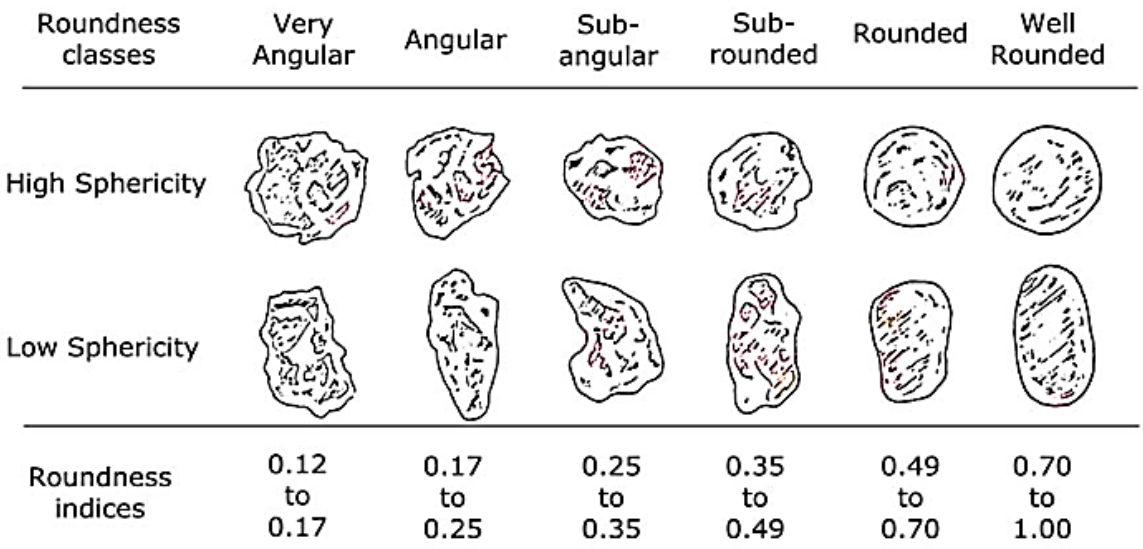

Figure I.4: Chart for estimating the roundness based upon comparisons with particles of known roundness. [7]

I-5-The uses of sand in modern Industry:

I-5-1-Industrial Sand:

Industrial sand is a term normally applied to high purity silica sand products with closely controlled sizing. For industrial and manufacturing applications, deposits of silica yielding products of at least 95% SiO_2 are preferred. Silica sand deposits are most commonly surface-mined in open pit operations [8], but dredging and underground mining are also employed. Extracted ore undergoes considerable processing to increase the silica content by reducing impurities. It is then dried and sized to produce the optimum particle size distribution for the intended application. [9]

I-5-2-Filtration and Water Production:

Tap water filtering and wastewater management both pass through a complex route of cleaning and filtering, which is aided by the use of industrial sand. Uniformity in grain shapes and grain size distributions allows a safe and efficient bed operation to remove contaminants in both drinking water and wastewater [8]. Silica is also the perfect filtration and water production material because it is chemically inert and will not react to acids. [9] It does not react to volatile organics, solvents, or any contaminant.

I.5.3-Glass production:

In the production of glass, there is both the need and requirement for silica to be chemically pure (composed of over 98% SiO_2), of the appropriate diameter (a grain size of between 0.075 mm and 1.18 mm), and color (must contain between 0.025% and 0.04% Fe_2O_3) [8]. These requirements are extremely specific and technical; and this is because the silica must be hard, able to resist high temperatures, and maintain a consistent appearance as a finished product.

I.5.4-Metal Casting:

Industrial sand is an essential part of the ferrous and non-ferrous foundry industry. Metal parts ranging from engine blocks to sink faucets are cast in a sand and clay mold to produce the external shape, and a resin bonded core that creates the desired internal shape. Silica's high fusion point (1760°C) and low rate of thermal expansion produce stable cores and molds compatible with all pouring temperatures and alloy systems [10]. Its chemical purity also helps prevent interaction with catalysts or curing rate of chemical binders. Following the casting process, core sand can be thermally or mechanically recycled to produce new cores or molds.

I.5.5-Oil and Gas Recovery:

Known commonly as proppants, or "frac sand," industrial sand is pumped down holes in deep well applications to prop open rock fissures and increase the flow rate of natural gas or oil. In this specialized application round, whole grain deposits are used to maximize permeability and prevent formation cuttings from entering the well bore [10]. Silica's hardness and its overall structural integrity combine to deliver the required crush resistance of the high pressures present in wells up to 2,450 meters deep. Its chemical purity is required to resist chemical attack in corrosive environments.

I.6 - The silica minerals:

The silica minerals, with an overall composition SiO_2, include many polymorphs Quartz is the most common member, occurring both in a trigonal low-temperature form (α-quartz) and a hexagonal high-temperature form (β-quartz). Other important silica polymorphs are β-tridymite, β-cristobalite, coesite and stishovite. The stability fields of some silica polymorphs are shown in **(Figure I.5)** [11].

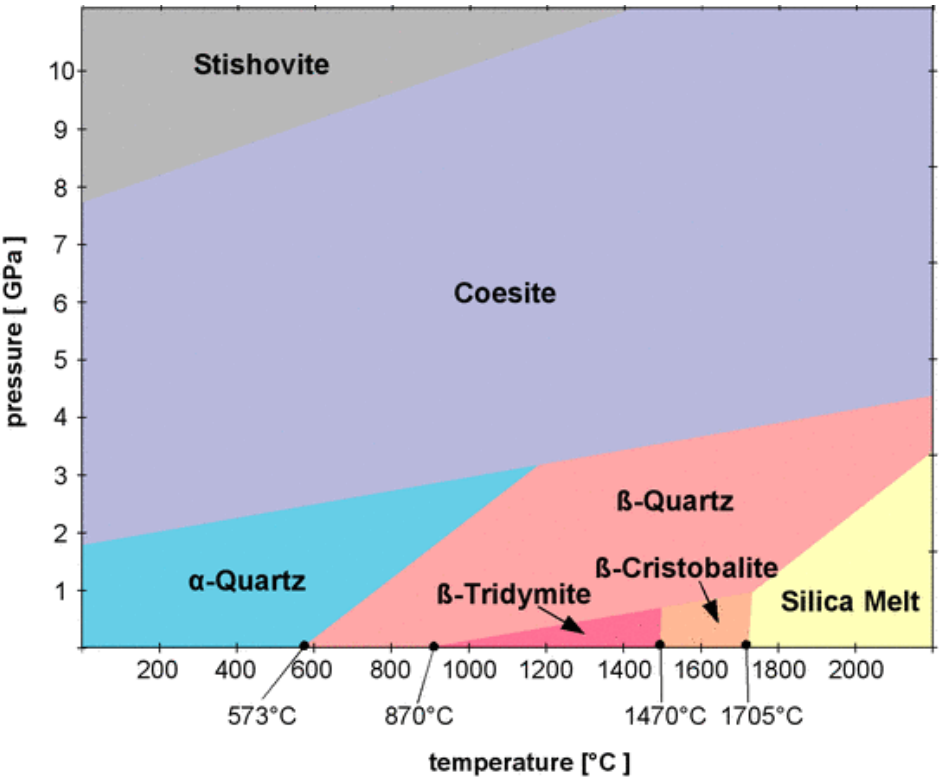

Figure I.5: The stability fields of some silica polymorphs [11]

From all the silica minerals shown above, this part focuses only on quartz because of its high presence in sand, and specifically α-quartz.

The mineral α-quartz comprises about 13% of the earth's crust and is the second most abundant mineral. the structure of quartz consists of an infinite three-dimensional framework of linked SiO_4^{-4} tetrahedra (**Figure I.6)**. [12] Each corner of a tetrahedron is shared with another one and we can only count it as one half per tetrahedron, resulting in an overall oxygen content of 4 × 1/2 = 2 and one silicon per tetrahedron, i.e, a molecular composition SiO_2. [11]

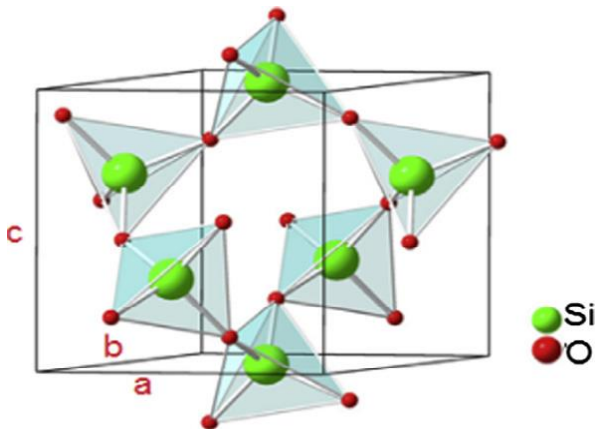

Figure I.6: three-dimensional framework of linked SiO_4^{-4}. [13]

I.6.1- General Properties of quartz:

1-Mohs Hardness:

Hardness Scale is defined loosely as resistance to indentation or abrasion. Quantitative tests for hardness can be made under a microscope using a diamond indenter and are an important part of the mineralogy of opaque ore minerals. The average geologist studies merely relative hardness, expressed by the resistance offered by a smooth surface of a mineral to scratching by a sharp edge on a material of known hardness. Around 1800 the German mineralogist **Friedrich Mohs** devised a relative scale that compares the hardness of some standard minerals **(Table I.3)** and this scale is still used universally. [11]

Table I.3: Moh's hardness scale [11]

Talc	Gypsum	Calcite	Fluorite	Apatite	Feldspar	Quartz	Topaz	Corundum	Diamond
$Mg_3Si_4O_{10}(OH)_2$	$CaSO_4 \cdot 2H_2O$	$CaCO_3$	CaF_2			SiO_2	$Al_2SiO_4(F,OH)_2$	Al_2O_3	C
1	2	3	4	5	6	7	8	9	10

2-Cleavage:

Cleavage is used to describe the planes within a mineral with weak bonding. A mineral can easily be split along these planes and cleaves/breaks into specific shapes **(Figure I.7)** based on the mineral structure. [14] We describe cleavage based on how well the mineral cleaves. Perfect cleavage occurs if the mineral breaks into continuous planes that are smooth enough to reflect light. Quartz basically has no cleavage. [11]

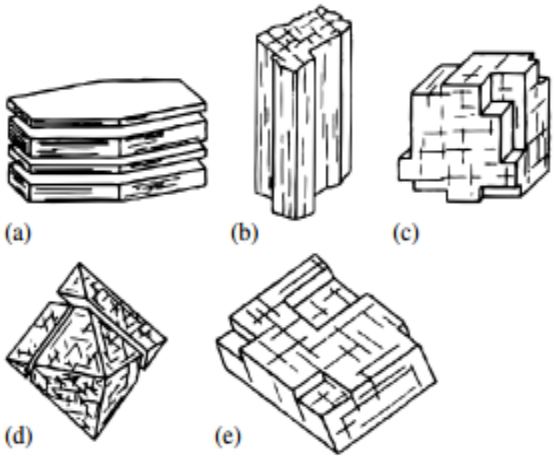

Figure I.7: Examples of cleavage in minerals. (a) Single cleavage causing a crystal to break up into flakes as in mica [11]

3-Fracture:

Many mineral crystals (e.g., quartz) show only poorly defined cleavage or none at all. When such crystals are struck they break on generally irregularly oriented curved surfaces decided more by the stress distribution in the crystal at the time of rupture than by the atomic, Quartz however has conchoidal fracture. [11]

4-Color:

The color of a mineral as directly observed can be so characteristic as to be an important aid in identification, but it can also be misleading. Most minerals, even the rock-forming silicates in which isomorphous series are present, can show a bewildering variety of colors. In general, color by itself is insufficient to permit identification, but it can be useful when taken together with other properties. Quartz occurs in many colors depending on the nature of the impurities it contains. [14]

5-Streak:

Many minerals show a characteristic color when reduced to a fine powder, regardless of the color they show in a bulk specimen. An example is hematite, which can range from red to metallic gray in hand specimens but always produces a dark red-brown powder on grinding. This property is called streak. [14]

6- Luster:

The term luster is used to describe the character of the light reflected from the surface of a mineral and depends on the refractive index. Terms in common use refer the luster of a mineral to that of some common material (e.g., metallic luster, waxy luster, earthy luster, and so on). The main division is into metallic and nonmetallic and the latter can have many different expressions. [15] [11]

The luster of some minerals is as follows:

Table I.4: The luster of some minerals. [11]

Metallic	Submetallic	Adamantine	Resinous	Vitreous	Earthy
silver	magnetite	diamond	gypsum	quartz	graphite

The table Below **(Table I.5)** sums up the most important properties of quartz.

Table 1.5: The general identification points for quartz [11]

Property	**Value**
Chemical Formula	SiO_2
Hardness	7
Luster	vitreous
Streak	white
Cleavage	none
Fracture	conchoidal
Crystal System	trigonal, hexagonal
Specific Gravity (g/m^3)	2.65
Color	clear, white, red, orange, yellow, green, blue, purple, brown, black
Index of Refraction	1.544 - 1.5553
Unit cell dimensions	a = 4.913Å b = 4.913Å c = 5.405Å

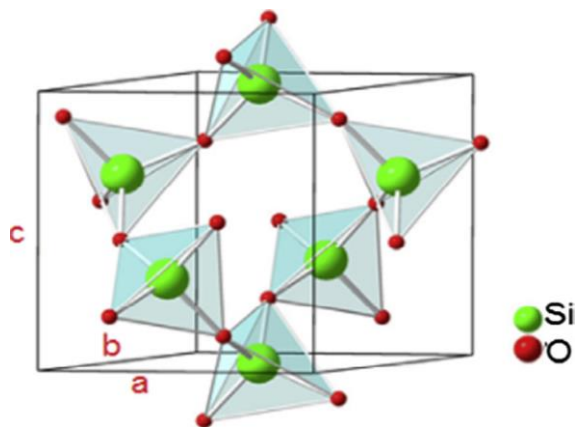

I.6.2-From Beta-Quartz to Alpha-Quartz:

The hexagonal β-quartz exists only above 573 ˚C. Upon cooling, tetrahedra become tilted, resulting in a less symmetrical trigonal structure (α-quartz) (**Figure I.8)**. This transformation involves only slight displacements of atoms, with no breakage of bonds, and is therefore instantaneous and reversible. [15]

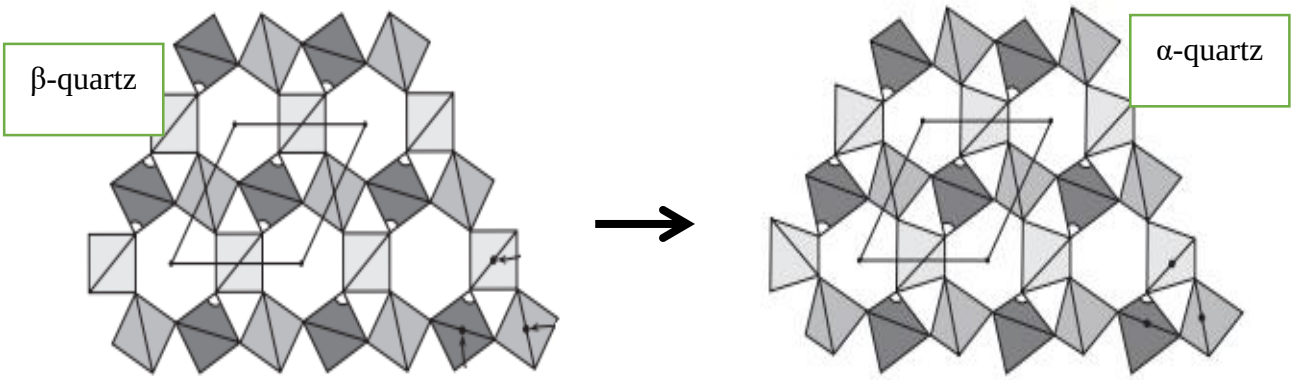

Figure I.8: From β-quartz to α-quartz [11]

I.7.1-The optical properties of quartz:

1-Birefringence:

Like many other minerals, quartz shows a very interesting property called birefringence or double refraction. This phenomenon is well known from calcite: when a clear calcite rhombohedron is put on a newspaper, one can see a double image of the letters. A single ray of light is split up into two rays while it passes the rhombohedron. Birefringence is present in many crystallographically non-isometric (non-cubic) materials and is absent from amorphous materials, isometric (cubic) minerals, and liquids. [14] [15]

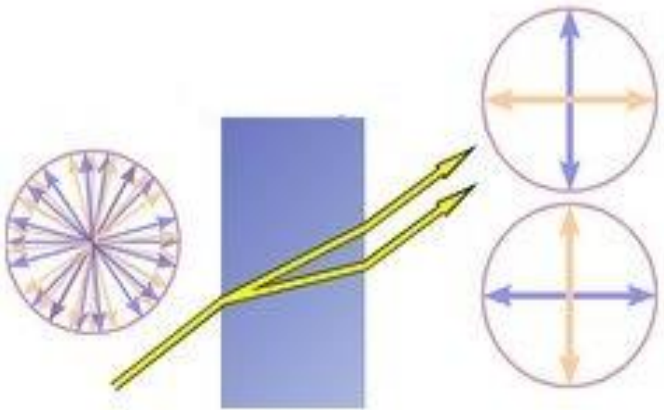

Figure I.9: Birefringence [14]

The optical axis in quartz corresponds to the c-axis of the unit cell, so there is no birefringence when light passes the crystal from tip to tip. The maximum birefringence occurs when the light passes perpendicular to the optical axis (**Figure I.10** with the amount of birefringence greatly exaggerated). Light that passes the crystal along the c-axis will also not be split into two rays of opposite polarization. [14]

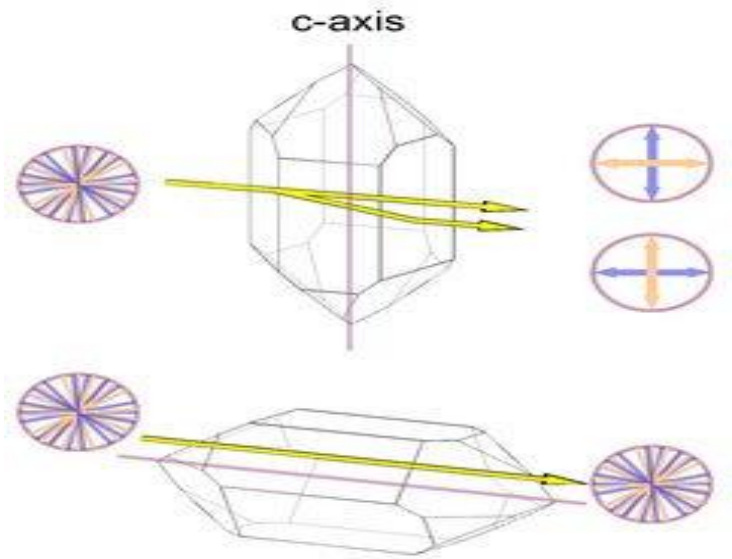

Figure I.10: Birefringence and Polarization [14]

2-Dispersion

The coefficient of dispersion is a measure of how much the refractive index of a substance depends on the wavelength of the light. Quartz has a low coefficient of dispersion and thus cannot be used as a diamond imitation. In optical apparatus dispersion needs to be kept as low as possible, for example to avoid chromatic aberrations of a camera lens. Note that dispersion is not a phenomenon confined to anisotropic crystals, it can be observed in isotropic crystals and non-crystalline substances as well, for example ordinary glass, or water (causing the rainbow). [15]

The following table (**Table I.6)** of refractive indices for both the ordinary n_o and the extraordinary ray n_e, with colors given instead of wavelengths:

Table I.6: Indices of refraction for both the ordinary n_o and the extraordinary ray n_e

	Red	**Yellow**	**Green**	**Blue**	**Violet**
n_o	1.5409	1.5442	1.5471	1.5497	1.5582
n_e	1.5499	1.5533	1.5563	1.5589	1.5677

3-Dichroism

A transparent substance whose color depends on the direction of the light passing through it is called pleochroic. If it changes between two colors it is called dichroic [15]. Pure quartz is colorless and cannot be dichroic, but some of its colored varieties show a weak dichroism:

natural citrine: yellow/bright yellow

smoky quartz: yellow-brown/red-brown

amethyst: gray- or blue-violet/red-violet

ametrine: only the amethyst sectors: gray- or blue-violet/red-violet

prasiolite: yellow-green/blue-green

4-Piezoelectricity

In 1880, Pierre and Jacques Curie observed that a pressure exerted on a small piece of quartz caused an electrical potential between deformed surfaces **(Figure I.11)**, and that application of a voltage effected physical displacements. Thus, the piezoelectric (or pressure electric) effect was discovered. [17]

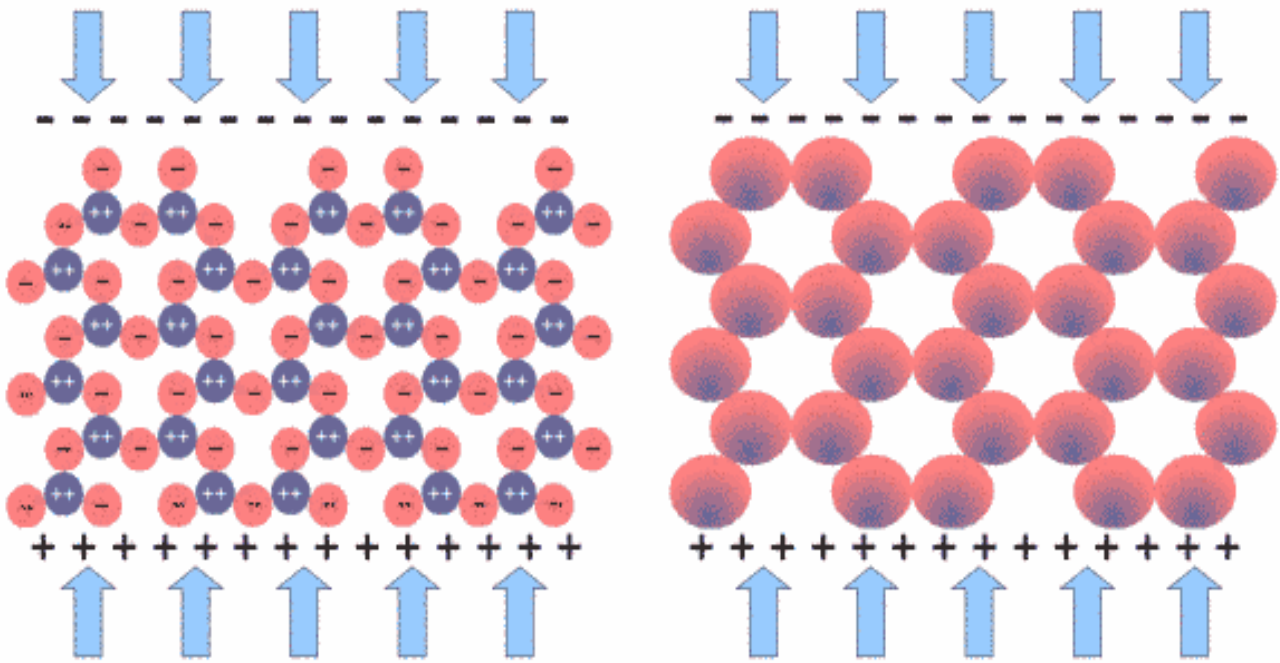

Figure I.11: The electrical potential between deformed surfaces [15]

I-7-2-Applications:

There are all kinds of situations where we need to convert mechanical energy (pressure or movement of some kind) into electrical signals or vice-versa. Often we can do that with a piezoelectric transducer. In ultrasound equipment, a piezoelectric transducer converts electrical energy into extremely rapid mechanical vibrations, so fast, in fact, that it makes sounds, but ones too high-pitched for our ears to hear. These ultrasound vibrations can be used for scanning, cleaning, and all kinds of other things. In a microphone, we need to convert sound energy (waves of pressure traveling through the air) into electrical energy, and that's something piezoelectric crystals can help us with. Simply stick the vibrating part of the microphone to a crystal and, as pressure waves from your voice arrive, they'll make the crystal move back and forth, generating corresponding electrical signals. [17]

In a quartz clock or watch, the reverse-piezoelectric effect is used to keep time very precisely. Electrical energy from a battery is fed into a crystal to make it oscillate thousands of times a second. The watch then uses an electronic circuit to turn that into slower, once-per-second beats that a tiny motor and some precision gears use to drive the second, minute, and hour hands around the clock-face. Also some printers inkjets squirt their syringes using electronically controlled piezoelectric crystals. [17]

Chapter II

Samples gathering and Experimental methods

II-1- Introduction:

This chapter is dedicated to explain the basics of the experimental methods and instruments used in the examination of sand samples. The methods covered in this chapter are X-Ray diffraction (XRD) and Fourier-transform infrared spectroscopy (FTIR).

II-2- The samples gathering:

The sand samples were taken from regions in Algeria/El-oued province (**figure II.1**). The samples S1, S2 and S3 were picked from dunes located in the south of the El-Oued area and sample S4 from the north of El-Oued region **(figure II.2)**.

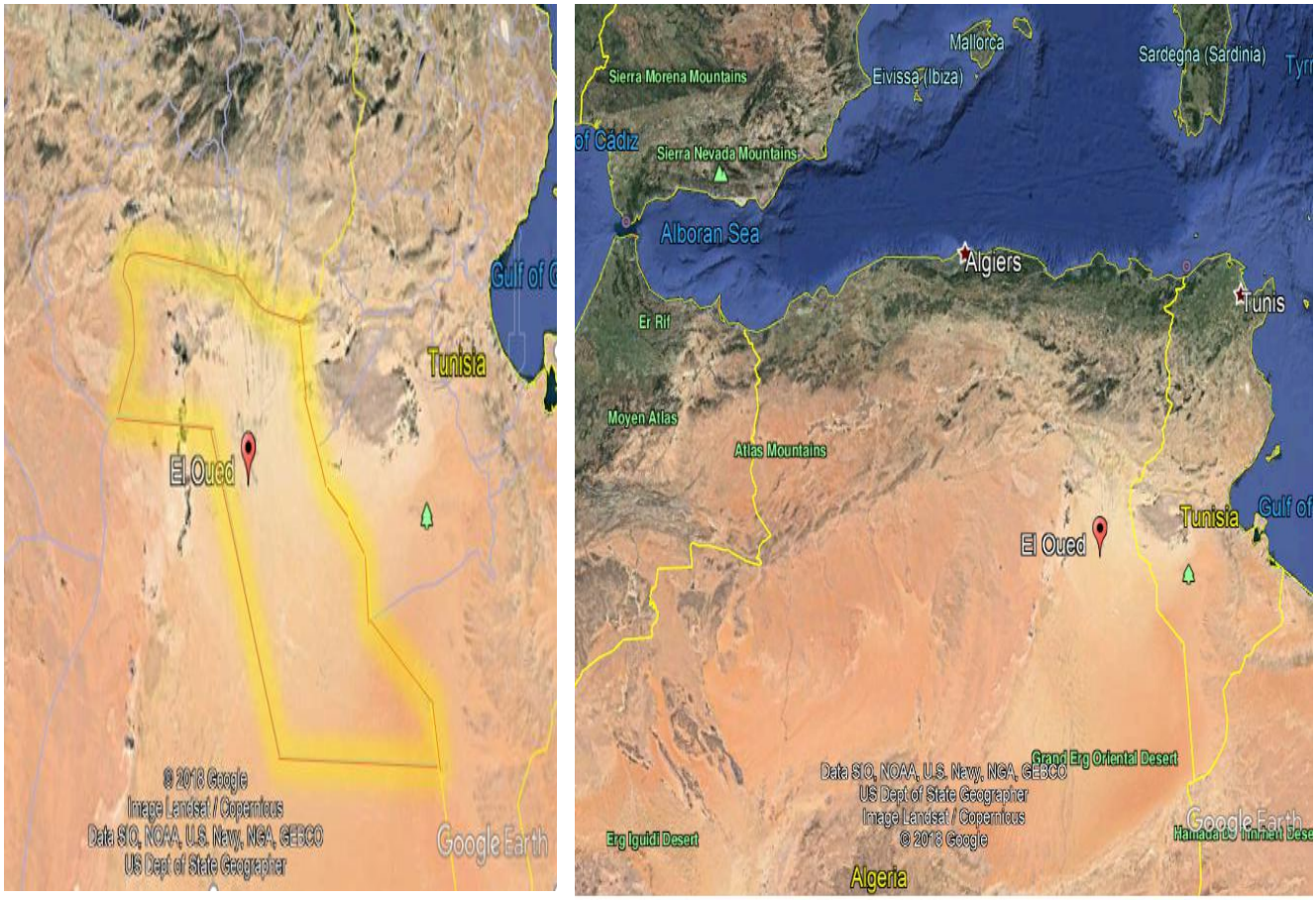

Figure II.1: The location of El-oued province in Algeria

Both the dunes and the region are perfectly located by the following coordinates:

S1 (33° 8'31.18"N , 6°51'12.42"E) **S2 (33° 8'28.93"N , 6°51'15.37"E)**

S3 (33° 8'34.02"N , 6°51'15.74"E) **S4 (33°42'36.96"N , 6°33'53.00"E)**

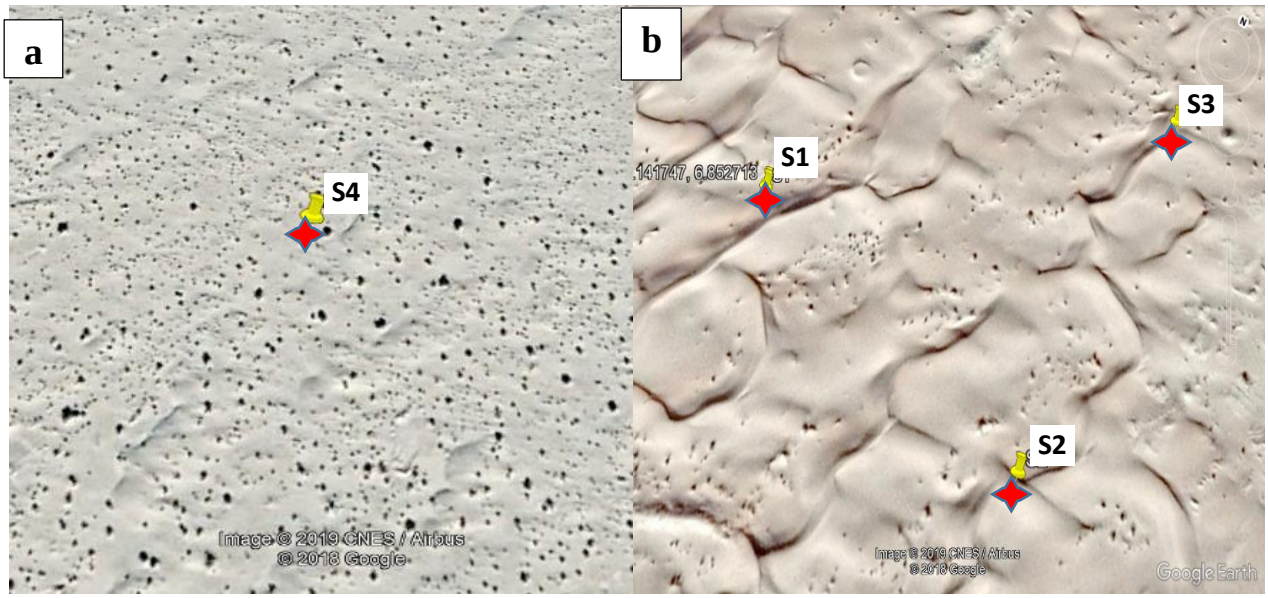

Figure II.2: (a) The location of the region where **S4** was picked and (b) the locations of the dunes that the samples **S1**, **S2** and **S3** were taken from as viewed by google earth.

These regions were carefully chosen to be away from any industrial contamination, and here are photos **(Figure II.3)** for the samples locations to support our claim.

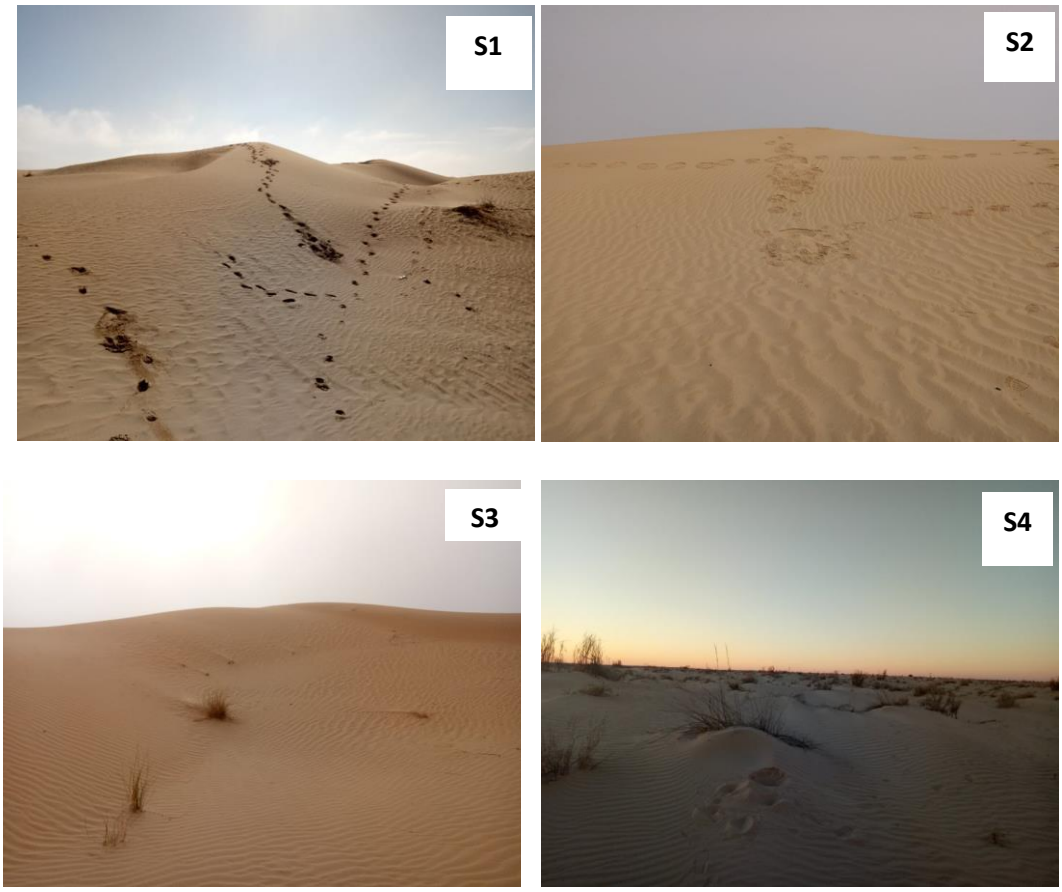

Figure II.3: Actual photos of the regions and dunes where the four samples were picked.

II-3- Experimental methods:

II-3-1-Fourier-transform infrared spectroscopy (FTIR):

The Analysis of infrared spectra can tell us what molecules are present in a sample, [20] this is why infrared spectroscopy is useful. There are several types of infrared spectrometers in the world, but the most widely used one is FTIR (Fourier Transform Infrared), which is the focus here. [19]

II-3-1-1- Infrared theory:

Naturally all molecules vibrate according to their vibration modes, but with very small amplitudes. If a photon frequency matches the vibration frequency of the molecule, then the molecule will respond to its oscillation. In other words, if a photon has just the necessary energy to take the molecule to a higher excited state **(figure II.4**), then it will get absorbed, and its energy will be transformed into vibrational energy. [20]

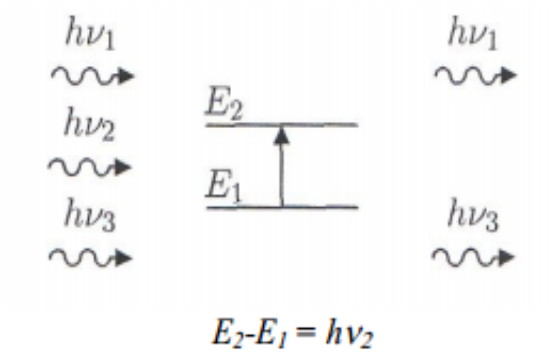

Figure II.4: A molecule's energy levels excited by a photon

The only photon that can be absorbed is the one of energy $h\nu_2$, that is equal to the transition energy (E_2-E_1). The absorbance of photons by the molecules leaves a trace on the transmittance spectrum (absorption band). Each frequency at which this absorption happens is characteristic to the molecule structure. [18]

II-3-1-2-Types of Molecular Vibrations:

1- Stretching or bonding vibrations:

In this case only the bonds lengths alter. this type can be subdivided into symmetric and anti-symmetric stretching **(Figure II.5)** [20]

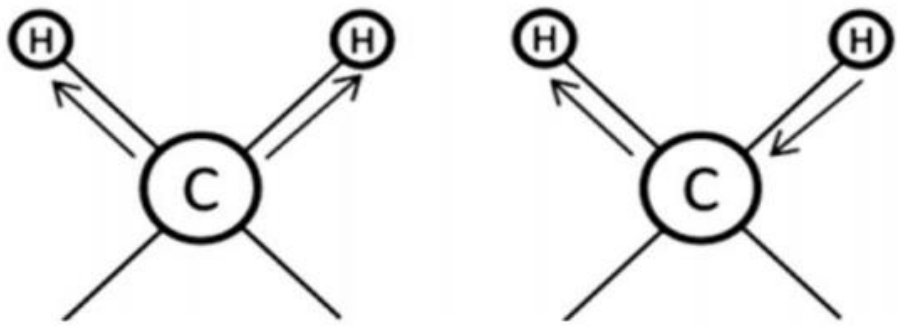

Figure II.5: symmetric and asymmetric stretching [19]

2- Bending or deformation vibrations:

This type Alters the bond angles, while the bond lengths remain unchanged, they can be subdivided into in-plane and out-of-plane modes, these modes are often referred to as twisting, wagging, and rocking vibrations. **(Figure II.6)** [21]

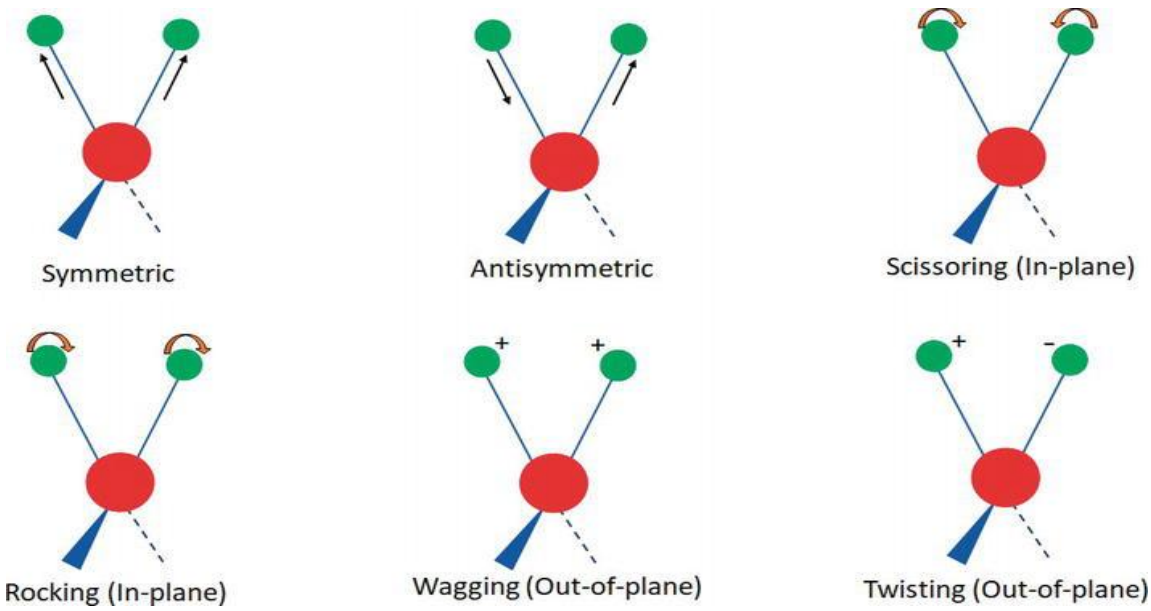

Figure II.6: Bending vibrations [21]

II-3-1-3- The electromagnetic radiation absorption:

The electromagnetic radiation is composed of electric and magnetic waves called the electric vector and the magnetic vector. These two waves undulate in planes mutually perpendicular to each other, and move through space in a third direction perpendicular to the planes of undulation. It is the

interaction of the electric vector with matter that leads to the absorbance of the EM. Each absorption range of the electromagnetic radiation corresponds to a certain electronic transition or molecular movement **(Table II.1).** [18]

Table II.1: A part of the electromagnetic spectrum [18]

Visible & UV >14,000 cm^{-1}	**Near IR** 14,000 to 4000 cm^{-1}	**Mid-Infrared** 4000 to 400 cm^{-1}	**Far Infrared** 400 to 4 cm^{-1}	**Microwaves** < 4 cm^{-1}
Electronic Transitions	Molecular Vibrations	Molecular Vibrations	Molecular Vibrations	Molecular Rotations

II-3-1-4- Infrared instrumentation:

At the heart of every FTIR is an optical device called an interferometer. A diagram of an interferometer is shown in **Figure II.7**. interferometer or "interference meter," measures the interference pattern between two light beams. The light from an infrared source is shown entering the interferometer from the left in **Figure II.7**. The interferometer splits the single light beam into two light beams. The interferometer then causes the two light beams to travel different paths, which are denoted D1 and D2 in **Figure II.7**. After the two light beams have traveled their different paths they are recombined into one beam, and then the light beam leaves the interferometer. [19] [20]

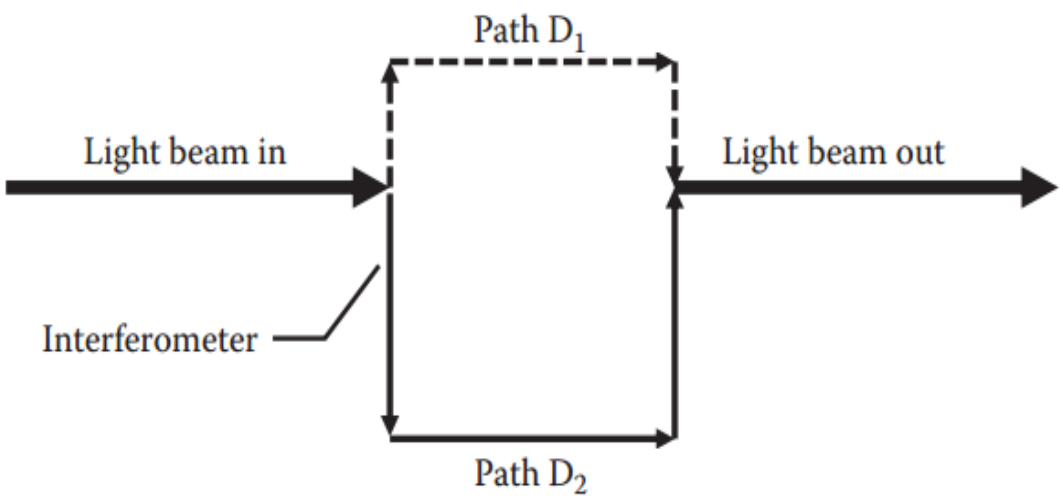

Figure II.7: Interferometer [18]

There are a number of interferometer designs used by FTIR manufacturers. The oldest and perhaps the most common type of interferometer in use today is the Michelson interferometer. It is named after Albert Abraham Michelson (1852–1931) **(Figure II.8)** who first built his interferometer in the 1880s. [20]

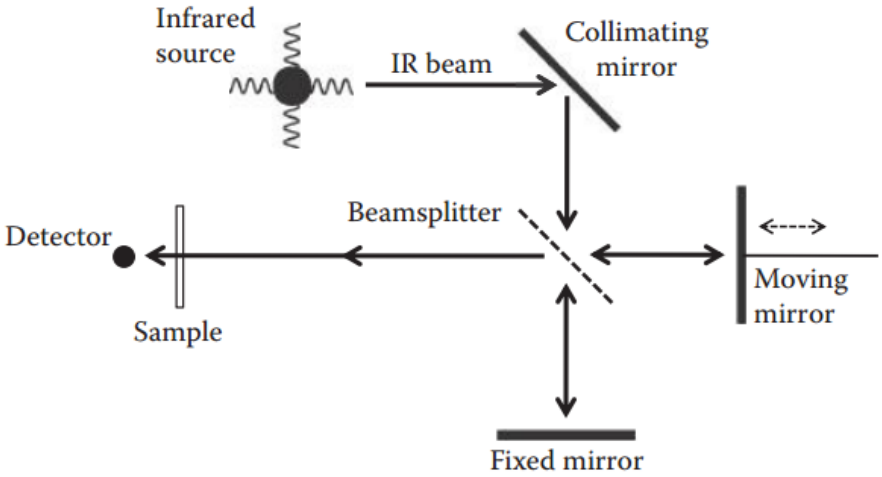

Figure II.8: Albert Abraham Michelson interferometer [18]

II-3-1-5- The Infrared spectrum:

The infrared spectrum is a plot of measured infrared light intensity versus a property of light is called an infrared spectrum. An example of an infrared spectrum is shown in **Figure II.9**. By convention the x-axis of an infrared spectrum is plotted with high wavenumber to the left and low wavenumber to the right. Note in **Figure II.9** that 4000 cm^{-1} is to the left and 500 cm^{-1} is to the right, and that the spectrum is plotted in transmittance units, which measure the amount of light absorbed by a sample. As you can see in the figure the peaks point up and their tops denote wavenumbers at which significant amounts of light were absorbed by the sample. [20]

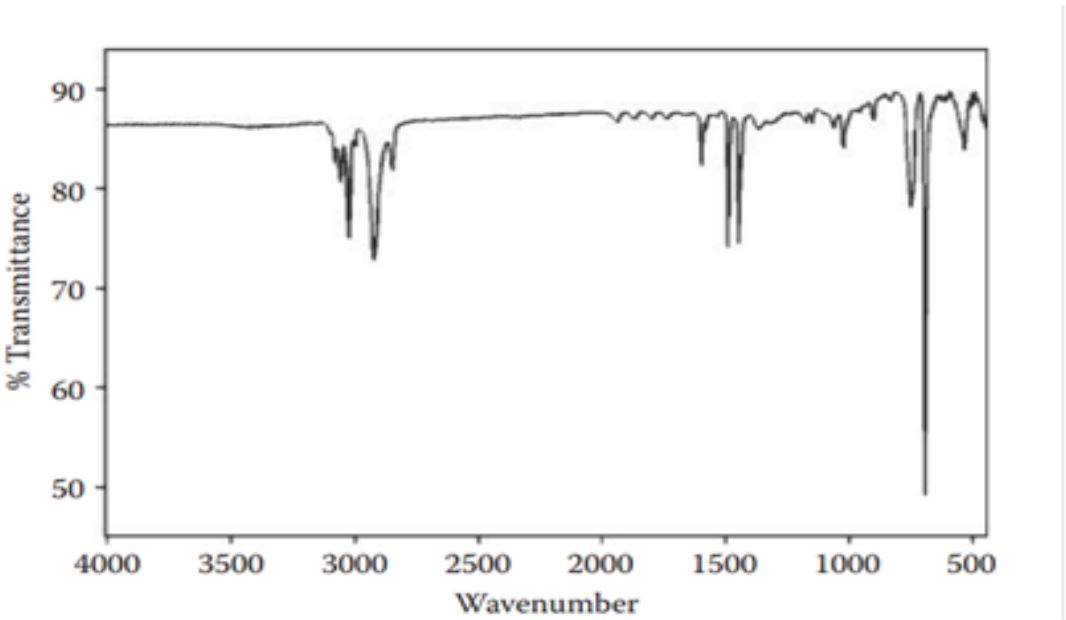

Figure II.9: Infrared transmittance Spectrum

II-3-2- X-ray diffraction (XRD):

II-3-2-1- A brief history:

The notion that crystals have a lattice-based structure and that the basic building block is the unit cell was introduced in the eighteenth century. At that time the analysis of crystals was based on visual inspection, on detailed examination with a hand lens or at best a light microscope. However, visible light, with wavelengths between 400 and 700 nm, is far too coarse a probe to investigate crystal structures where information is on the scale of atoms and interatomic distances, i.e,1-5 A (1 A ˚ = 0.1 nm). [22] However, in the early twentieth century new techniques were developed to study crystal lattices, providing a tool for determining structural parameters and largely confirming the concepts about unit parallelepipeds, lattice structure, and symmetry suggested more than 100 years earlier. With the discovery of X-rays by C.W. Rontgen in 1895, the stage was set for analyzing crystals at an elementary level, and this research produced information about the solid state. Then in 1912 the famous diffraction experiment of Max von Laue established that X-rays are waves and that the suspected internal lattice structure of crystals indeed existed.

II-3-2-2- The source of X-rays:

It was found that when electrons were accelerated in an electric field and collided with a metal anode, a very high-energy radiation was emitted. At the time, he was unable to explain the origin of this radiation (hence the name ‘‘X-rays’’), and an explanation had to wait until more was known about the structure of atoms. It became clear that accelerated electrons with sufficiently high energy could displace electrons from within the inner electron shells (e.g., a K shell electron) of an atom **(Figure II.10)**. This is because the energy of the electrons within the inner shells is close to, but slightly less than, the energy of the accelerated electrons. An electron from a higher shell immediately fills the electron hole, and the excess energy is released as a photon. The energy, and hence the wavelength, corresponds to the particular electronic transition of a given atom. These high-energy photons have short wavelengths λ (λ = hc/eV, where h is the Planck constant, c the speed of light, e the charge of the electron, and V the accelerating voltage) in the range 0.1-5 A, which make them ideal for crystal structure studies, and are called X-rays. [11]

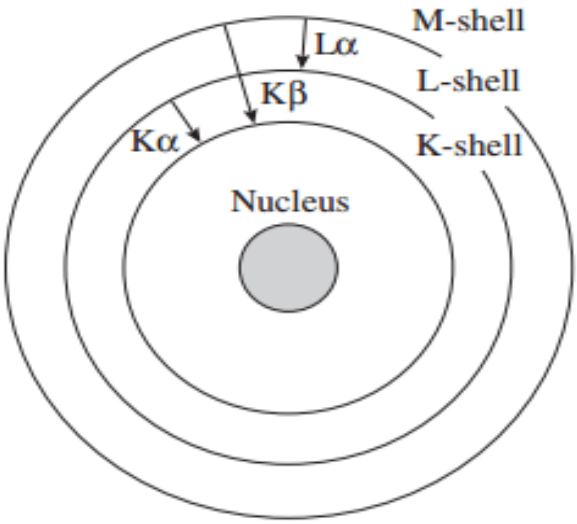

Figure II.10: Energy transitions of inner shell electrons. [11]

For most applications X-rays are produced by an X-ray tube, powered by an X-ray generator. **Figure II.11** shows a schematic diagram of a modern X-ray tube. [11] It consists of an evacuated glass tube in which electrons are released by heating a tungsten filament (just as in a normal light bulb). By applying a voltage, the electrons are then accelerated in a field to 40-50 keV and collide with an anode metal. [24]

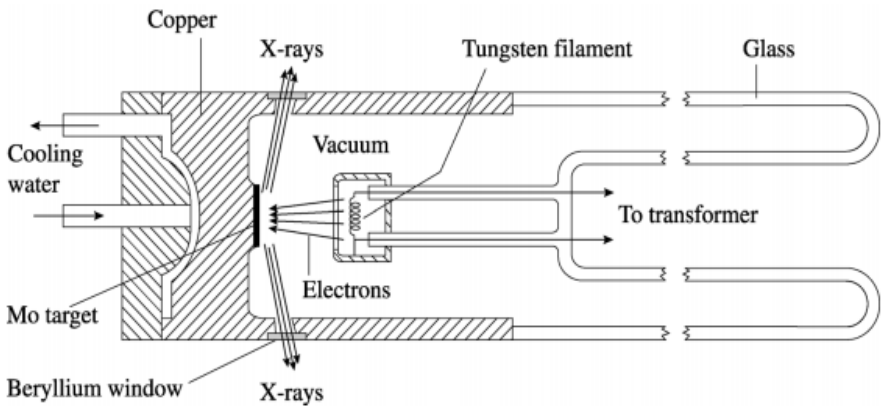

Figure II.11: Generation of X-rays in a modern X-ray tube. [11]

Owing to the energy transitions in the anode, X-rays are produced and leave the tube through beryllium windows that have relatively low absorption. In an X-ray tube most of the energy of the electrons is not converted to X-rays but to heat, and thus it is necessary to cool the anode metal, usually with water. [22]

II-3-2-3- Bragg equation:

its known that crystals consist of stacks of lattice planes (**Figure II.12)**, and X-rays penetrate many hundred. In the figure Two waves, which are initially in phase, reach a crystal. The first (1) diffracts (reflects) on the lattice plane (hkl) on the surface, the second one (2) on the parallel plane below at a distance d = AC. [11] [22] The angle of incidence to the lattice plane is θ. The second wave has a longer path (PD = BC +CD), before the two waves establish a new wave front AD.

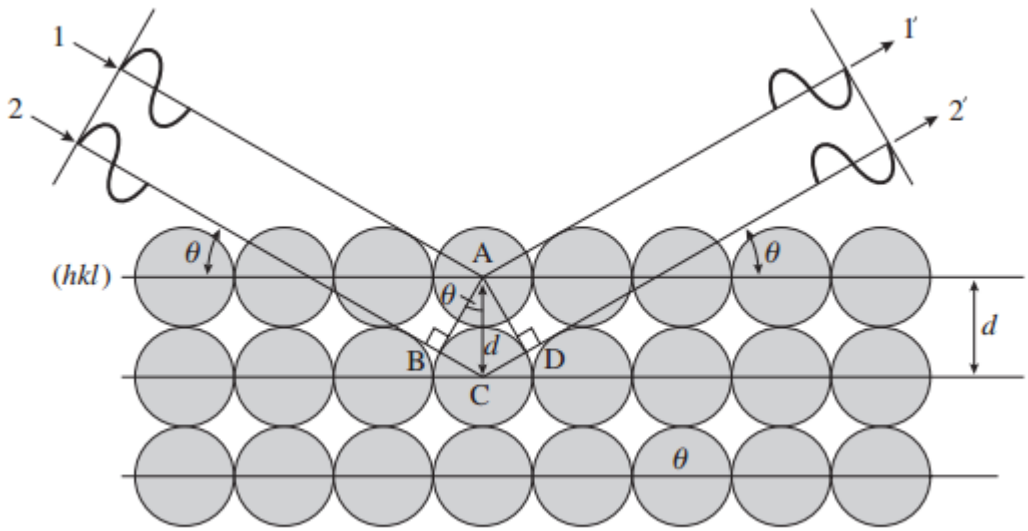

Figure II.12: Derivation of Bragg's equation, explaining diffraction as reflection on a stack of lattice planes with an interplanar spacing d. [11]

We can easily establish a relationship (triangle ABC) sin θ = BC/AC, and correspondingly for diffraction, where the path difference has to be a multiple of the wavelength to produce constructive interference. [22] The bragg's equation is given as follows:

$$\boldsymbol{PD = 2d \sin \theta = n.\lambda} \qquad \textbf{(2.1)}$$

where λ is the wavelength, θ is the angle of incidence and reflection, and n is an integer. The relationship is known as the Bragg equation (or Bragg's law) and was formulated in 1913 by the father and son team W.H. and W.L. Bragg. Diffraction can be viewed as reflection on lattice planes with reflection angles θ determined by the spacing of lattice planes.

Bragg's law has two conditions:

1. The lattice planes (hkl) must be in a reflection orientation between the incident and diffracted X-ray waves.

2. Diffraction occurs at a specific angle that is determined by the d-spacing of the lattice planes.

These conditions are seemingly very straightforward but are not easy to satisfy experimentally. If we aim a monochromatic X-ray at a crystal in some arbitrary orientation, the Bragg conditions are not satisfied and no diffraction occurs. A crystal has to be rotated to bring a particular lattice plane hkl into a reflecting position, and then the diffraction angle has to be adjusted to fit with the spacing of the lattice plane d_{hkl}. Modern computer-controlled X-ray goniometers can help to alleviate some of these problems, and they are used for special applications. However, a significant experimental advancement came in 1916, when P. Debye and P. Scherrer had the ingenious idea to use powders instead of single crystals.

II-3-2-4- The powder method:

In a powder consists of many randomly oriented small crystals or ‘‘crystallites’’. There will always be some crystallites with lattice planes in the right orientation to diffract (i.e., satisfying the first Bragg condition), and therefore rotation is not necessary. A powder irradiated with monochromatic X-rays of known wavelength will produce diffracted X-rays lying on cones with an opening angle 4θ (i.e., an angle 2θ to the primary X-ray beam). We can intersect these cones with a photographic film, usually mounted in a cylindrical ‘‘Debye-Scherrer’’ camera, [11] [22] and image a set of concentric rings **(Figure II.13).** After exposure, the film is unrolled, developed and diffraction angles can be measured as distances between dark lines

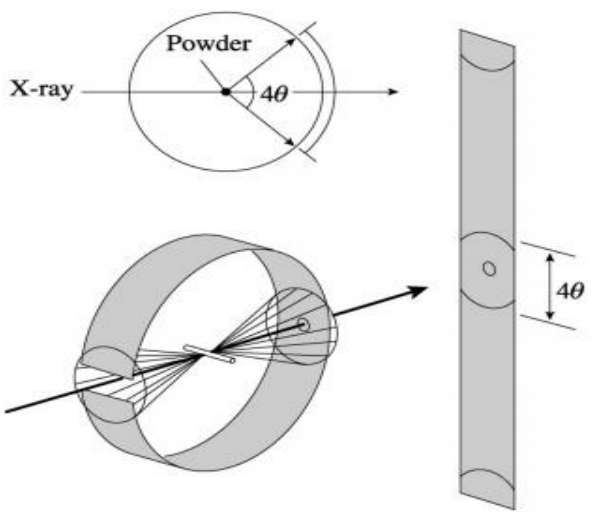

Figure II.13: In the powder method diffractions from crystallites lie on cones around the primary beam with an opening angle 4θ. [11]

.

Today the most popular powder method uses a powder diffractometer. The powder is suspended on a flat disk, and the reflections are scanned with an electronic detector **(Figure II.14)** that digitally

records the intensity as a function of diffraction angle, as is shown for a sample of cubic halite in **(Figure II.15).**

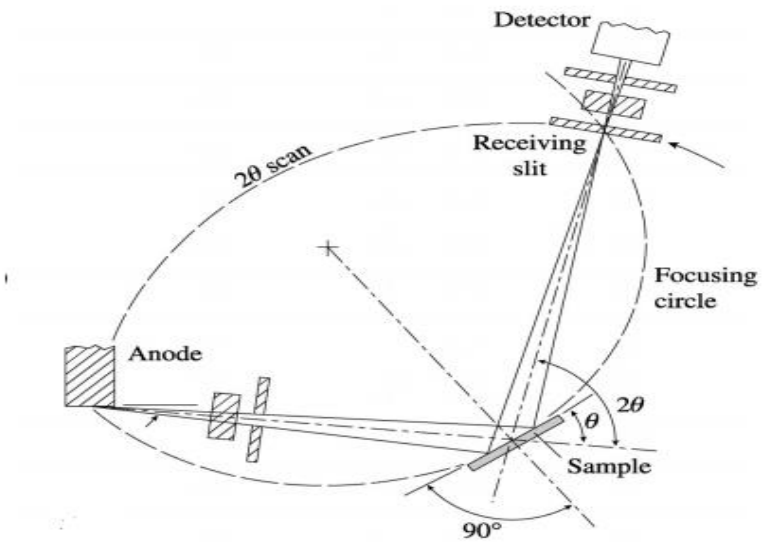

Figure II.14: A diffractometer scans the 2θ angle range with an electronic detector to record diffractions from a flat sample. [11]

Each peak corresponds to diffractions from different lattice planes. The detector rotates with an angular velocity of 2θ, whereas the sample rotates at a velocity θ to maintain the reflection condition for the surface of the sample. It means that, at all diffraction angles, those lattice planes (and only those) that are parallel to the sample surface are diffracting. [22]

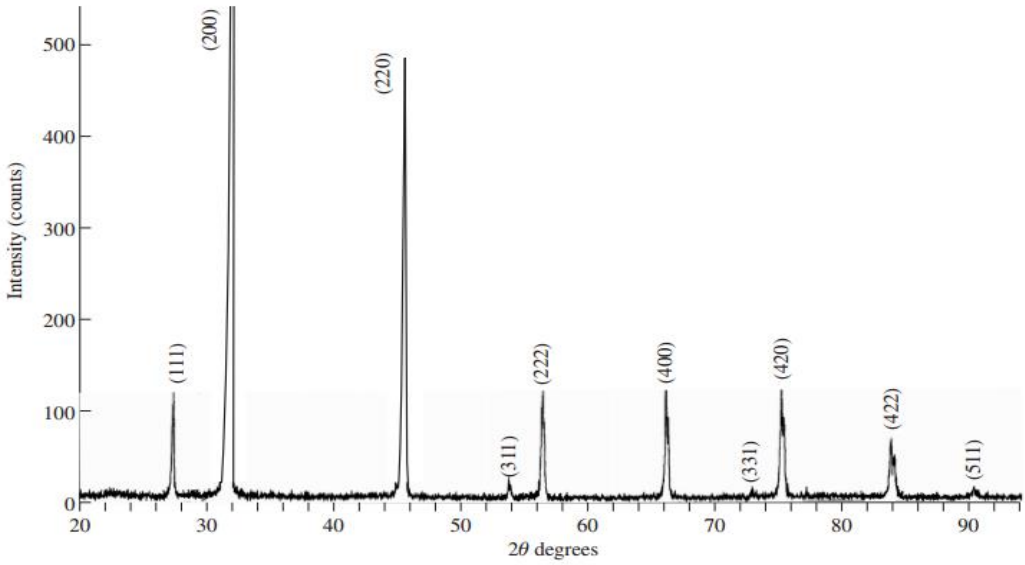

Figure II.15: Diffractometer pattern of halite. Each peak is assigned a lattice plane on which reflection occurs. 2θ angles are indicated. Kα copper radiation is used (λ = 1.5418 A). [11]

II-3-2-4-The match software:

"Match" is an easy to use software for phase identification from powder diffraction data. It compares the diffraction pattern of your sample to a database containing reference patterns in order to identify the phases which are present. Additional knowledge about the sample like known phases, elements or density can be applied easily.

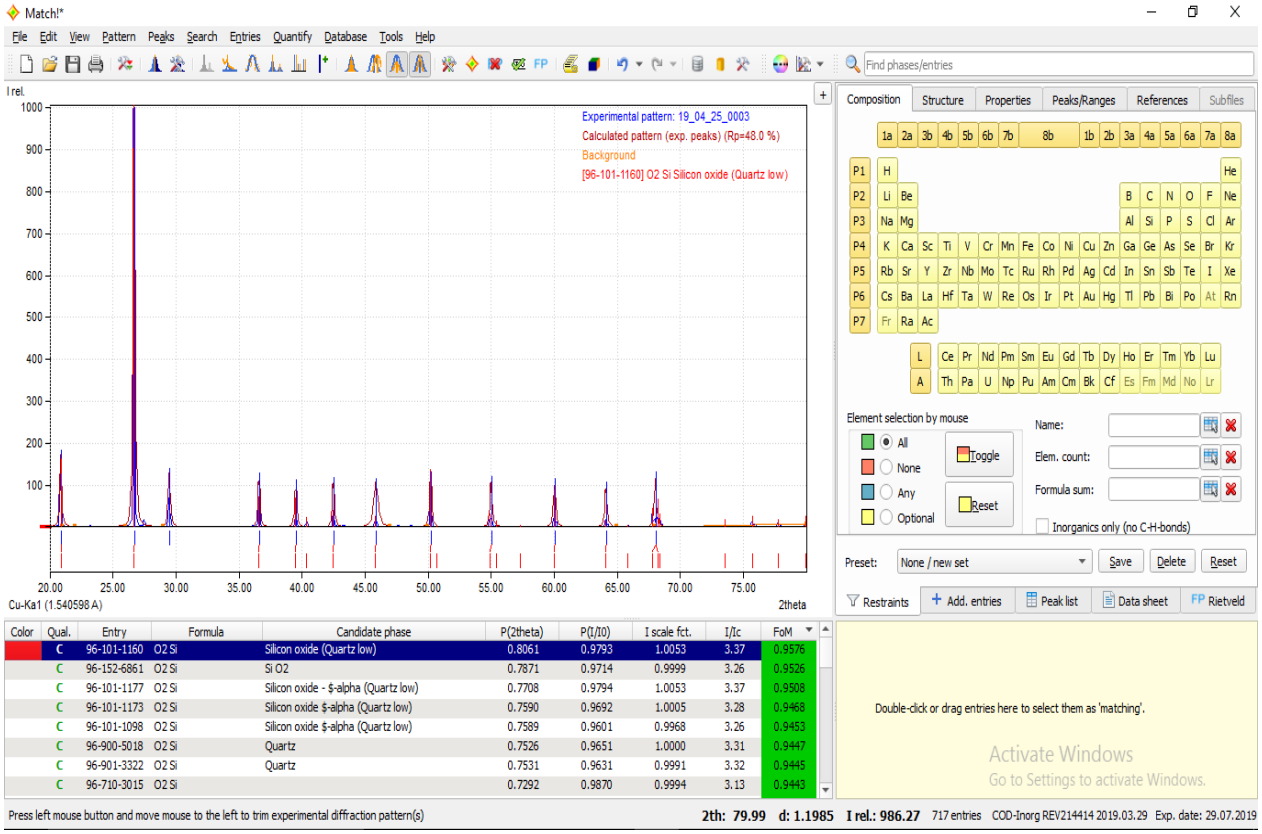

Figure II.16: The interface of Match software

Chapter III

Results and discussion

III-1-Introduction

This chapter presents and discusses the results of both FTIR and the XRD analysis, and then ends the study with a conclusion.

III-2-FTIR analysis

III-2-1-KBr Disc sample preparation

A KBr disc **(Figure III.1)** involves mixing of dried KBr powder and finely ground sample. The **KBr** sample mixture forms a clear disc when put under high pressure using a hydraulic press. Only 4 mg of sample and 200 mg is needed for this sample preparation. The sample must be ground to fine particles using an agate mortar and pestle **(Figure III.2)**.

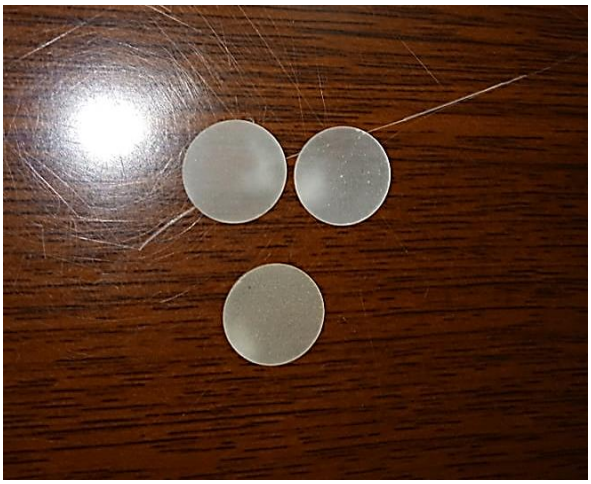

Figure III.1: KBr discs prepared for the **FTIR**

Figure III.2: A Mortar and pestle

III-2-2-Machine information

The FTIR machine was used is Shimadzu FTIR-8300 (**Figure III.3**) running under the spectral range (400 - 4000 cm^{-1}) the constituent bonds of the sand samples.

Figure III.3: Shimadzu FTIR-8300 machine

III-2-3-Results and discussion

The figures below represent the **FTIR** transmittance spectrum of El-oued's sand samples

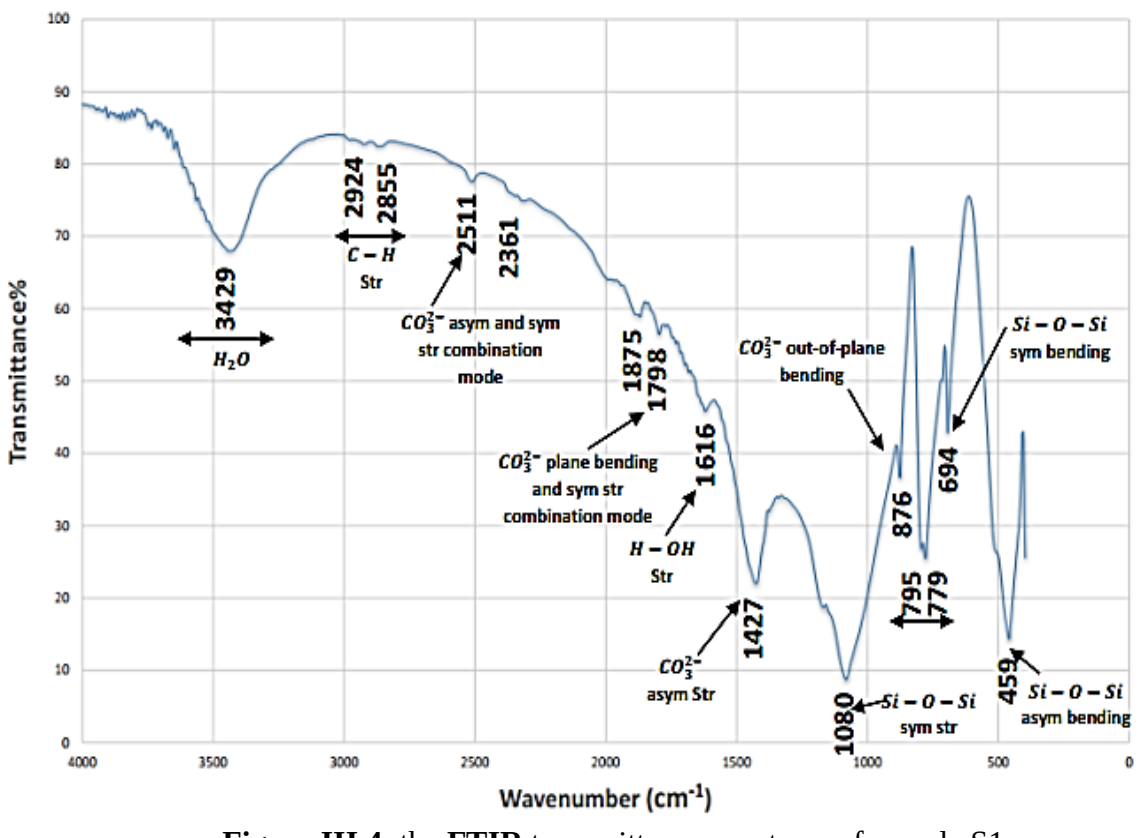

Figure III.4: the **FTIR** transmittance spectrum of sample S1

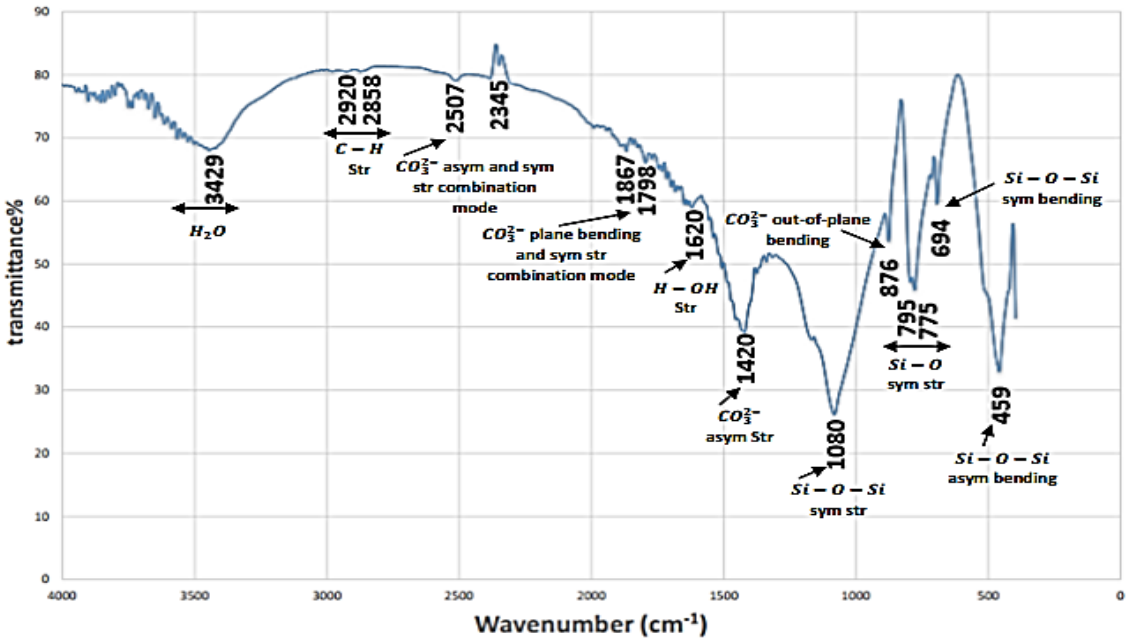

Figure III.5: the **FTIR** transmittance spectrum of sample S2

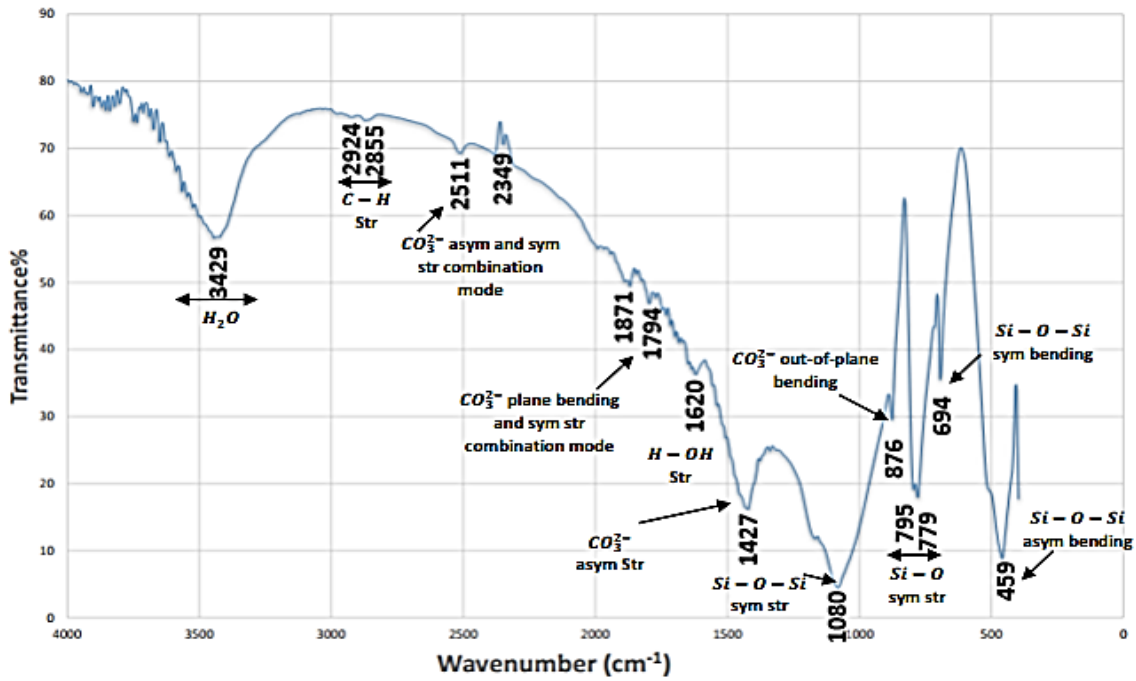

Figure III.6: the **FTIR** transmittance spectrum of sample S3

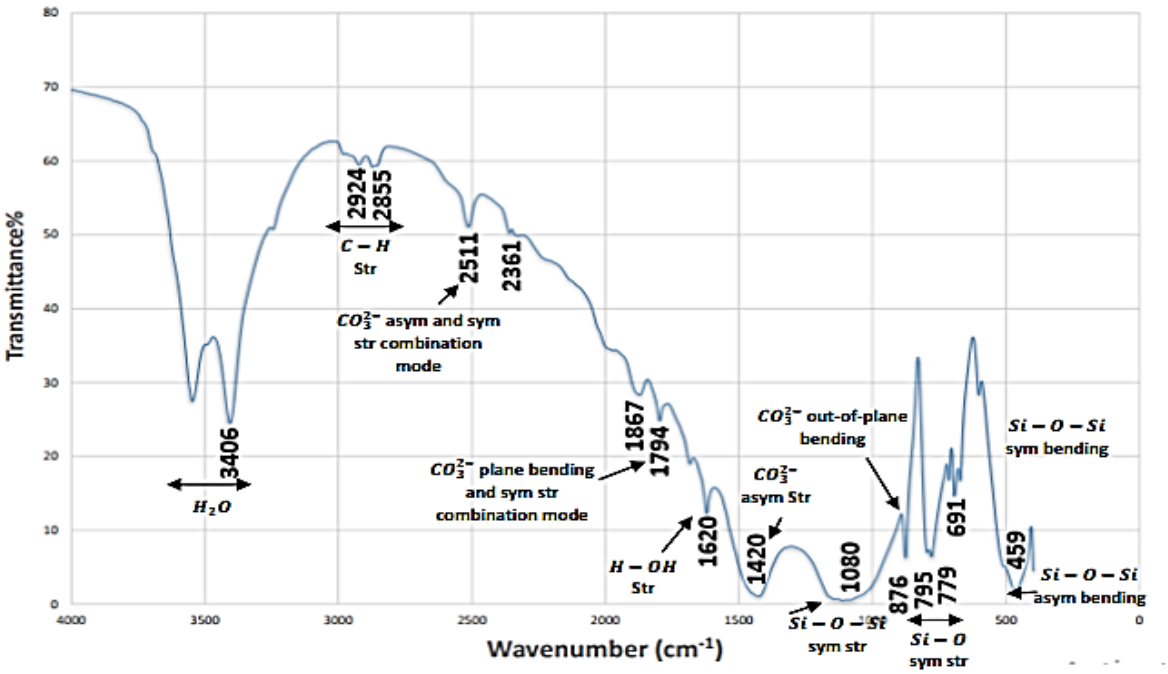

Figure III.7: the **FTIR** transmittance spectrum of sample S4

As seen above the FTIR spectrums obtained by examining of the El-Oued sand samples are show in **Figures (III.4, III.5, III.6, III.7)**. From the FTIR spectrums we can identify the main components of our samples. **Table III.1** summarizes the functional groups found in the sand. In the range of the high wavenumbers we see a high intensity absorption band at 3429 cm^{-1} which is due to stretching vibrations of hydroxyl groups (OH), a less intense band has been observed at 1616 cm^{-1}, which is due to the twisting of H-O-H .Also, three absorption bands have been observed at wavenumbers of 2511 cm^{-1}, which are due to $(CO3)^{-2}$ Asymmetrical and symmetrical stretching mode vibrations. The 1427 cm^{-1} wavenumber feature is due to doubly degenerate asymmetric stretching mode vibration, and the 876 cm^{-1} one corresponds to the C=O stretching mode vibration. These bands confirm the presence of calcite in our samples. A sharp absorption band at 1080 cm^{-1} has been observed and seems to fit with symmetrical stretching of Si–O–Si bond. In the spectrum range of 1080 – 400 cm^{-1} a strong band has been observed [23]. Symmetrical bands at 795 and 779 cm^{-1} have been observed and correspond to Si-O symmetrical bending vibration. These peaks confirm the presence of quartz. In addition, we observed other bands at 694 and 459 cm^{-1} which coincide with Si–O–Si symmetrical and asymmetrical bending, respectively. The presence of Si-O and O-Si-O vibrations in our sample again confirm the presence of quartz. The 694 cm^{-1} band indicates that the

quartz in our samples is crystalline. Thus, FTIR absorption spectrum exhibits only an absorption band characterizing quartz (SiO_2) and calcite ($CaCO_3$) compounds in our sand samples [19].

Table III.1: The functional groups found in the sand samples

Band (cm^{-1})	Bond (Vibration mode)	Compound
3429, 3406	$H-O-H$ (stretching vibration)	Water
2924 or 2920	$C-H$ (stretching vibration)	Organic Carbon
2855 or 2858	$C-H$ (stretching vibration)	Organic Carbon
2511or 2507	$(CO3)^{-2}$ (asymmetrical stretch and symmetrical stretching)	Calcite
1875, 1871 or 1867		Quartz
1798 or 1794	$(CO3)^{-2}$ (plane bending and symmetrical stretching combination mode)	Calcite
1620 or 1616	$H-OH$ (stretching)	Water
1427 or 1420	$(CO3)^{-2}$ (asymmetrical stretching)	Calcite
1080	$Si-O-Si$ (symmetrical stretching)	Quartz
876	$(CO3)^{-2}$ (out-of-plane bending)	Calcite
779,775	$Si-O$ (symmetrical stretching)	Quartz
694 or 691	$Si-O-Si$ (symmetrical bending)	Quartz
463 or 459	$Si-O-Si$ (asymmetrical bending)	Quartz

the FTIR results obtained by examining the sand samples of EL-Oued are almost identical. Also these results suggest the presence of a high purity degree quartz. On the other hand, other studies [15] showed that the Western Erg sand and the Ouargla sand in the Algerian Sahara have a considerable amount of Al_2O_3 and Fe_2O_3 [19]. The presence of the double absorption at 795 and 779 cm^{-1} is an indicator of the presence of the quartz in α-phase. This confirms what was said in the first chapter, quartz under the atmospheric pressure and relatively low temperatures exists in the α-phase, the crystallinity index (CI) of quartz in our sample is calculated by measuring the ratio between the absorbance of the bands 695 cm^{-1} and 795 cm^{-1} (A_{695}/A_{795}) [13], where the absorbance A_α at wavenumber α is given as:

$$A_{\alpha} = log\frac{T_0}{T} \qquad \textbf{3.1}$$

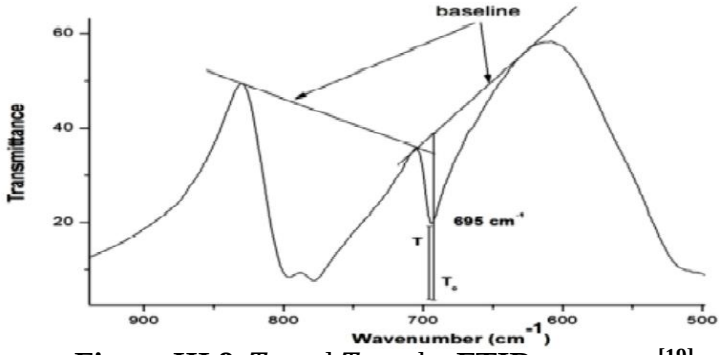

Figure III.8: T_0 and T on the **FTIR** spectrum[19]

where T_0 and T are illustrated in **figure III.8** :

The table **III.2** below presents calculated of quartz in all samples:

Table III.2: Sand crystallinity indices

Sample	695 (cm^{-1})		795 (cm^{-1})		A_{695}	A_{795}	CI $=A_{695}/A_{795}$
	T_0	T	T_0	T			
S1	58.67	43.34	65.33	26.67	0.132	0.390	0.34
S2	78.67	50	73.33	63.33	0.197	0.064	0.33
S3	54.67	38.67	66.67	20.67	0.150	0.510	0.30
S4	28	18	30	10	0.192	0.477	0.40

This high crystalline nature of quartz in our samples has encouraged to further our study with an XRD analysis.

III-2-XRD analysis:

III-2-1-Samples preparation:

Before processing the sand samples by the **XRD,** they first have to be grounded to fine particles (**Figure III.9)** using mortar and pestle, the necessity of this step is explained in chapter II.

Figure III.9: Sand powder

III-2-3-Results and discussion:

After exposing the four samples of El-Oued's sand to the x-rays, four diffraction spectrums were obtained. By analyzing these spectrums using the software "match", it was possible to identify dominant chemical compounds present in the sand samples.

The peaks appearing in the figures below at angles 2θ : 20.90°,26.71° , 36.63°, 39.54°, 42.52°, 45.90°, 50.23°, 55.02°, 60.06°, 64.13°, 68.06° correspond to quartz($\boldsymbol{SiO_2}$). Also the peaks at 29.50°, 48.80° and 73.70° are proof for the existence of calcite ($\boldsymbol{CaCO_3}$). The signal peak at 27.71° is hint for the presence of Wollastonite in S2.

The reflections at the distances d_{hkl} 4.2514 , 3.3372 and 1.5405 Å are a confirmation for the presence of α-quartz.

Also using the peaks data obtained by "Match" enabled us to calculate crystallite size of both quartz and calcite. The relation between the width full at half maximum (FWHM) of the most intense diffraction peak given by the software and the crystallite size (D) is given below by Scherrer's formula [23]:

$$D = \frac{K\lambda}{\beta \cos(\theta)} \qquad \mathbf{3.1}$$

where $\lambda = 1.540593$Å is the wavelength of the X-rays used, and $K = 0.96$, θ is the angle of diffraction and β is Full width at half maximum . [23]

As it was expected in The FTIR analysis, the XRD results of the four samples showed that El-Oued's sand contains high percentage of Quartz(SiO_2), however Calcite($CaCO_3$) only appeared in samples S1, S2 and S4.

Also by processing the XRD spectrums samples using "Match" software, we were able to determine the miller indices of each plane, the interplanar distances d and the peaks intensities.

Also by processing the XRD spectrums samples using "Match" software, we were able to determine the miller indices of each plane, the interplanar distances d and the peaks intensities. This information is shown in the tables below:

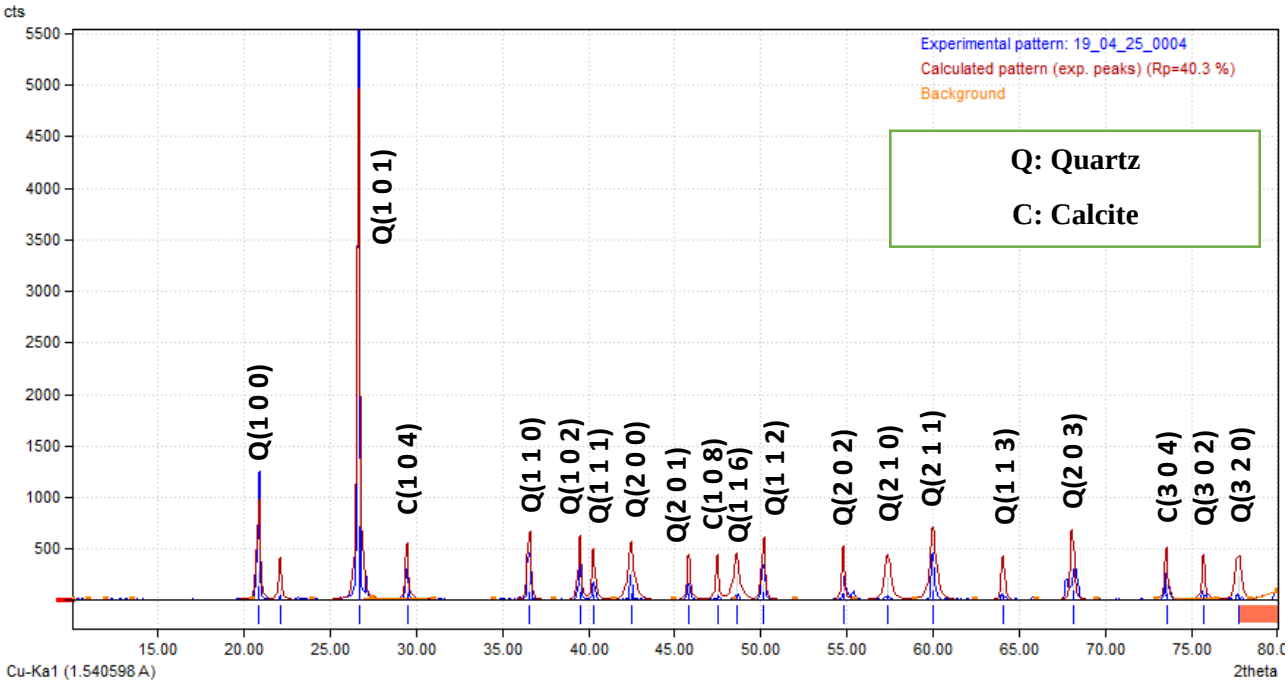

Figure III.10: XRD spectrum of S1

Table III.3: Structural properties of El-Oued's sand (S1)

(Diffraction angle) $2\theta\circ$	Interplanar distance($\dot{A}$)	Miller indices (hkl)			FWHM (deg)	Crystallite size(nm)	Mineral	intensity
20.88	4.2514	1	0	0	0.2000		Quartz	202.13
26.68	3.3380	1	0	1	0.2000	43,5663	Quartz	1000.00
29.48	3.0277	1	0	4	0.2000		Calcite	114.12
36.58	2.4542	1	1	0	0.2000		Quartz	132.78
39.52	2.2787	1	0	2	0.2000		Quartz	119.83
40.33	2.2346	1	1	1	0.2000		Quartz	96.34
42.50	2.1252	2	0	0	0.4000		Quartz	107.29
45.85	1.9773	2	0	1	0.2000		Quartz	97.78
47.50	1.9127	1	0	8	0.2000		Calcite	82.02
48.62	1.8711	1	1	6	0.4000		Calcite	85.90
50.18	1.8166	1	1	2	0.2000		Quartz	123.79
54.81	1.6736	2	0	2	0.2000		Quartz	100.75
57.41	1.6038	2	1	0	0.4000		Quartz	82.51
60.04	1.5396	2	1	1	0.4000		Quartz	138.97
64.09	1.4518	1	1	3	0.2000		Quartz	83. 91
68.13	1.3752	2	0	3	0.2000	51,1718	Calcite	136.81

73.58	1.2863	3	0	6	0.2000		Quartz	104.79
75.74	1.2548	3	0	2	0.2000		Quartz	88.29
77.76	1.2272	2	2	0	0.4000		Quartz	85.98

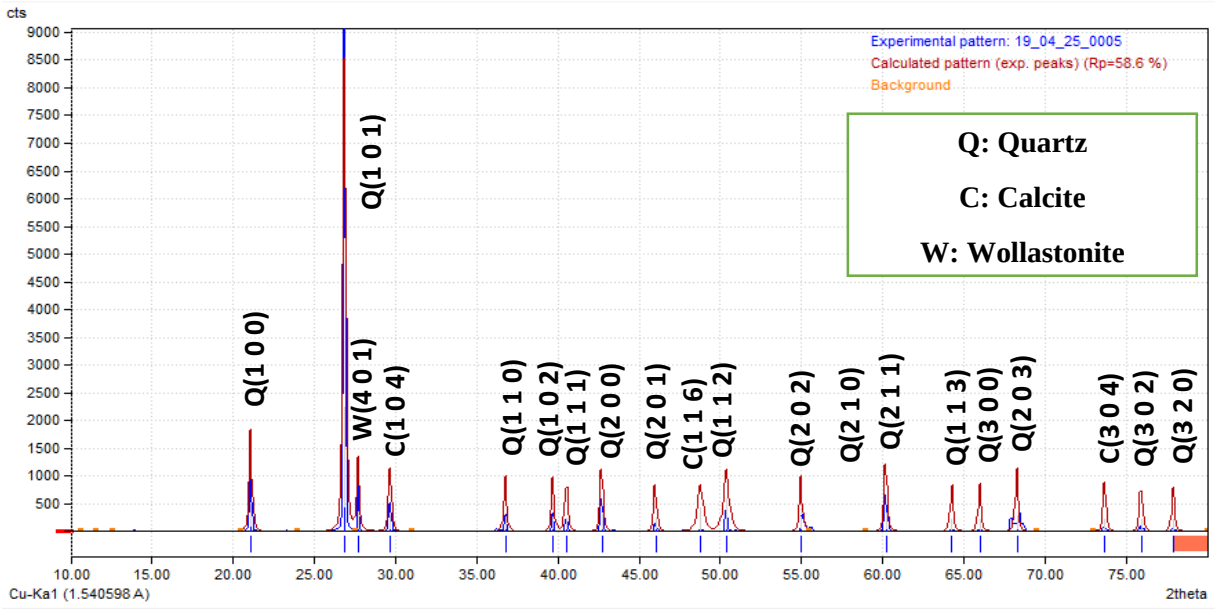

Figure III.11: XRD spectrum of (S2**)**

Table III.4: Structural properties of El-Oued's sand (S2**)**

(Diffraction angle) $2\theta\circ$	Interplanar distance($\dot{A}$)	Miller indices (hkl)			FWHM (deg)	Crystallite size(nm)	Mineral	intensity
21.10	4.2070	1	0	0	0.2000		Quartz	214.39
26.89	3.3130	1	0	1	0.2000	43,5854	Quartz	1000.00
27.71	3.2358	4	0	1	0.2000		Wollastonite	155.46
29.69	3.0068	1	0	4	0.2000	43,8821	Calcite	134.29
36.79	2.4409	1	1	0	0.2000		Quartz	116.88
39.72	2.2672	1	0	2	0.2000		Quartz	118.23
40.55	2.2229	1	1	1	0.2000		Quartz	113.17
42.72	2.1147	2	0	0	0.2000		Quartz	136.82
46.03	1.9703	2	1	0	0.2000		Quartz	105.37
48.80	1.8646	1	1	6	0.4000		Calcite	98.15
50.40	1.8090	1	1	2	0.4000		Quartz	129.78
55.00	1.6682	2	0	2	0.2000		Quartz	116.13
60.22	1.5354	2	1	1	0.2000		Quartz	146.01
64.28	1.4479	1	1	3	0.2000		Quartz	98.73
66.00	1.4143	3	0	0	0.2000		Quartz	98.99
68.29	1.3724	2	0	3	0.2000		Quartz	134.08
73.70	1.2845	3	0	6	0.2000		Calcite	102.08
75.95	1.2519	3	0	2	0.2000		Quartz	103.39
77.93	1.2249	2	2	0	0.2000		Quartz	99.48

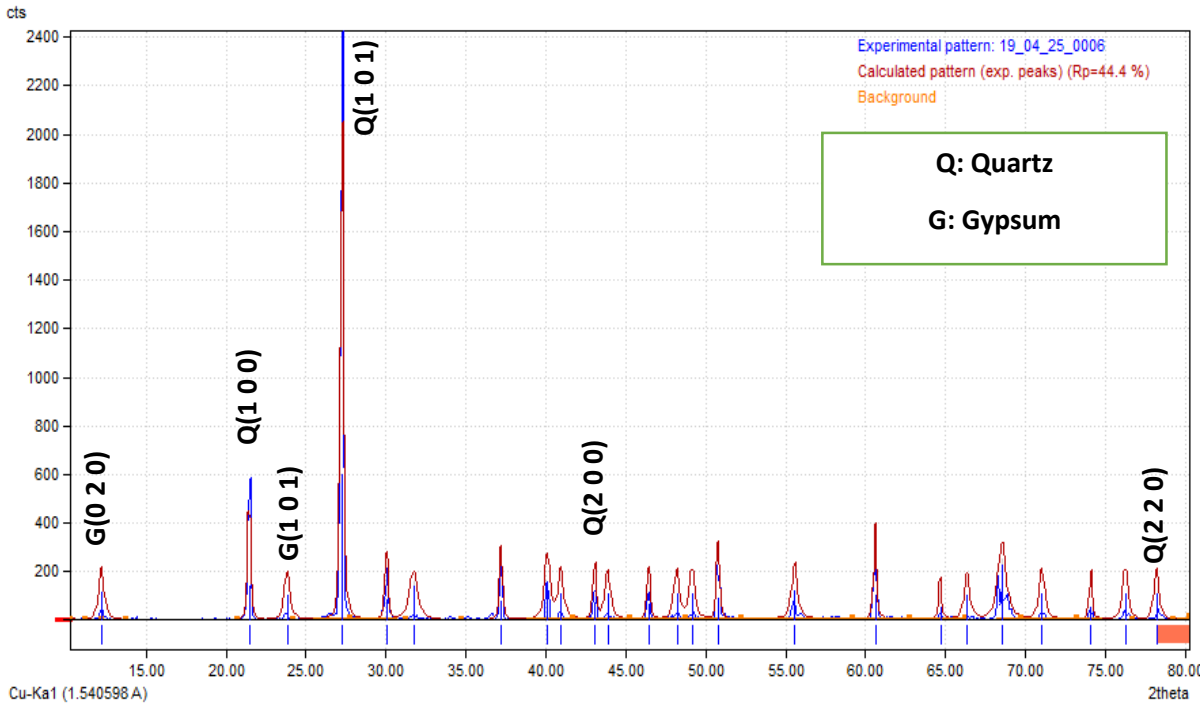

Figure III.12: XRD spectrum of **S3**

The third sample one of its kind, due to its odd peaks pattern, in this sample two peaks related to **Gypsum ($CaSO_4$. $2H_2O$)** were noticed, whereas these peaks didn't appear in the other samples. Also, unlike the other samples, in this spectrum fewer peaks related quartz and none of calcite appeared.

The only logical explanation of these observations is as follows:

the reason behind the presence of gypsum in this sample, is that it was taken from a region where there is a lot of traditional houses ruins, the essential building material of these building is gypsum and through weathering it was mixed with the surrounding sand.

The appearance of only few peaks related to quartz and calcite is due to the poor grounding of the sample. This made the chances of getting more atomic layers at angles that meet Bragg's equation too slim.

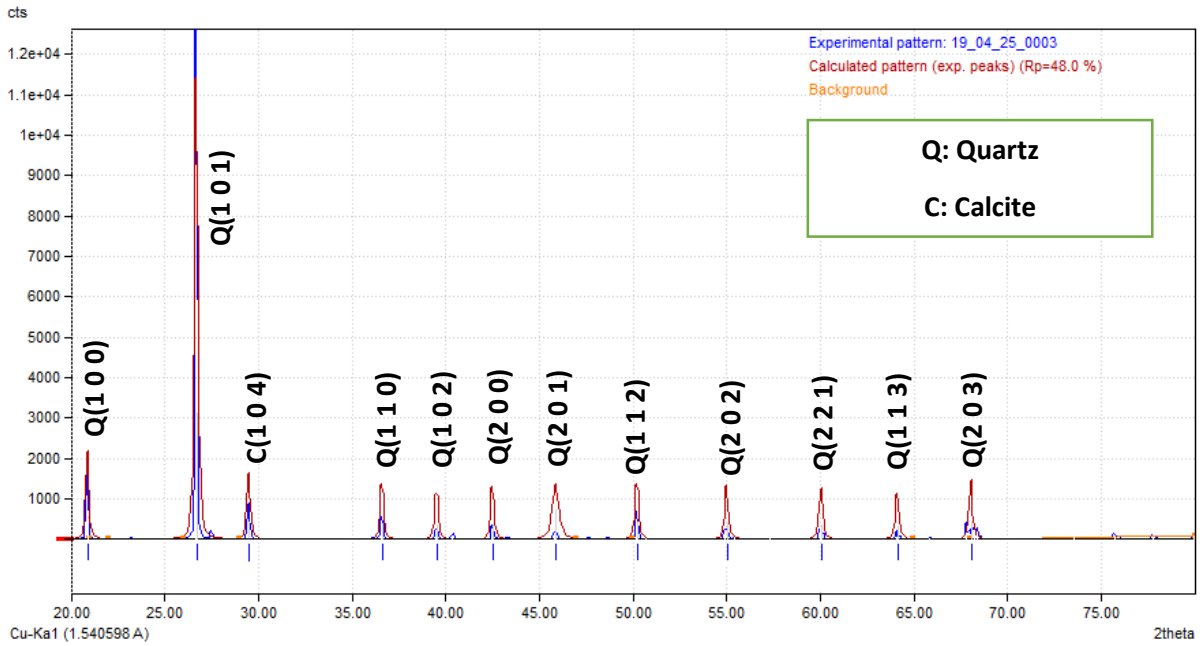

Figure III.13: XRD spectrum of S4

Table III.5: Structural properties of El-Oued's sand (S4**)**

(Diffraction angle) $2\theta\circ$	Interplanar distance($\dot{A}$)	Miller indices (hkl)	FWHM (deg)	Crystallite size(nm)	Mineral	intensity
20.90	4.2474	1 0 0	0.2000		Quartz	183.14
26.71	3.3344	1 0 1	0.2000	43,5745	Quartz	1000.00
29.51	3.0248	1 0 4	0.2000	43,8897	Calcite	139.69
36.63	2.4515	1 1 0	0.2000		Quartz	129.92
39.54	2.2775	1 0 2	0.2000		Quartz	113.22
42.52	2.1244	2 0 0	0.2000		Quartz	116.91
45.90	1.9757	2 0 1	0.4000		Quartz	114.83
50.23	1.8149	1 1 2	0.2000		Quartz	131.88
55.02	1.6677	2 0 2	0.2000		Quartz	120.58
60.06	1.5393	2 2 1	0.2000		Quartz	114.43
64.13	1.4510	1 1 3	0.2000		Quartz	108.04
68.06	1.3765	2 0 3	0.2000		Quartz	132.69

Also processing the data obtained by the XRD using the software "Match" enabled us to draw out some structural information of the materials composing El-Oued's sand, such as the unit cell dimensions (a, b, c), crystal system and the space group. The tables (**Table III.6 and Table III.7**) sum up all this information.

Table III.6: Structural information of Quartz in El-Oued's sand (S1,S2,S3,S4)

Chemical formula	SiO_2
Type	α-quartz
Molar mass (u.m.a)	60.08
Density (g/m^3)	2.66
Crystal system	Hexagonal
Space group	$P3_221$
a (Å)	4.7750
b (Å)	4.7750
c (Å)	5.3046

Table III.7: Structural information of Calcite in El-Oued's sand (S1, S2, S4)

Chemical formula	$CaCO_3$
Type	Calcite
Molar mass (u.m.a)	100.08
Density (g/m^3)	2.720
Crystal system	Hexagonal
Space group	$R\bar{3}c$
a (Å)	4.9844
b (Å)	4.9844
c (Å)	17.0376

The calculated values of quartz SiO_2 cell dimensions were so close to values given by the "ASTM" paper (01-085-0794) a =b= 4,9100 Å ,c= 5,4000 Å. For calcite $CaCO_3$ the values provided by the "ASTM" (01-083-1762) a =b= 4,9896 Å ,c= 17,0610 Å , were also very close to the calculated ones.

Sample 4 (S4) was intentionally picked from a region north El-Oued, and samples S1 and S3 from a region south El-Oued. From the results obtained by the FTIR method and the XRD method showed a high presence of quartz in all those samples, so basically in the light of the results we can tell that El-Oued's sand in the north and in the south is identical.

General conclusion

General conclusion:

The aim of our study was to enrich our background and reinforced the studies that has been conducted on El-Oued's sand. The most appealing thing about sand is its abundance. Sand covers vast areas of Algeria's surface. It also has a high minerals content like quartz. Quartz is magical mineral and has a wide range of applications and is used in too many modern industries such as building, glass making and electronics.

For the purpose of our study four samples were taken from different regions in El-Oued, to prepare these samples of the FTIR and XRD examination they were grounded and crushed to fine powders using a mortar and pestle.

To examine the samples by The FTIR method, a specific amount of KBr was added. The mixture KBr and sand powder was turned into a disc using a hydraulic press. These discs were exposed to an infrared radiation of a wavenumber spectral range (400 - 4000 cm^{-1}). Four spectrums were obtained and Each absorption band in these spectrums correspond to a certain chemical compound. By this way we have managed to determine the presence of compounds like water, Calcite and most importantly quartz. Moreover, we calculated the crystallinity indices of quartz and the results ordered from S1 to S4 were as follows: 0.34, 0.33, 0.30 and 0.40. These results encouraged us to further our study with the XRD method.

In the XRD method we had to make sure that samples are fine powders. The XRD spectrums obtained held the fingerprint peaks of both quartz (dominating), calcite (minority) and no trace of feldspar was found. Using the match software enabled us to determine and calculate the interplanar distances and miller indices, also we were able to calculate the crystallite size of both quartz and calcite. Using the same software "Match" we have drawn out information on the sand quartz and calcite like the Density, space group, unit cell dimension and the crystal system.

Our study can also furthered by the examination of other sand properties such as the thermal conductivity.

Appendix

A

S1 Match report

Match! Phase Analysis Report

Sample: 19_04_25_0004

Sample Data	
File name	19_04_25_0004.xye
File path	C:/Users/2fik-pc/Desktop/Important/المذكرة/xr
Data collected	May 30, 2019 00:51:45
Data range	10.010° - 80.010°
Original data range	10.000° - 80.000°
Number of points	701
Step size	0.100
Rietveld refinement converged	No
Alpha2 subtracted	No
Background subtr.	No
Data smoothed	No
2theta correction	0.01°
Radiation	X-rays
Wavelength	1.540598 Å

Matched Phases

Index	***Amount (%)***	***Name***	***Formula sum***
A	96.1	Silicon oxide Quartz low	O2 Si
B	3.9	Calcite	C Ca O3
	15.9	*Unidentified peak area*	

A: Silicon oxide Quartz low (96.1 %)	
Formula sum	O2 Si
Entry number	96-101-1160
Figure-of-Merit (FoM)	0.953841
Total number of peaks	35
Peaks in range	21
Peaks matched	17
Intensity scale factor	0.98
Space group	P 32 2 1 S
Crystal system	trigonal (hexagonal axes)
Unit cell	a= 4.9100 Å c= 5.4000 Å
I/Ic	3.37
Meas. density	2.660 g/cm³
Calc. density	2.654 g/cm³
Reference	Machatschki F, "Kristallstruktur von Tiefquarz", Fortschritte der Mineralogie **20**, 45-47 (1936)

B: Calcite (3.9 %)	
Formula sum	C Ca O3
Entry number	96-900-9669
Figure-of-Merit (FoM)	0.769244
Total number of peaks	38
Peaks in range	24
Peaks matched	6
Intensity scale factor	0.04
Space group	R -3 c
Crystal system	trigonal (hexagonal axes)
Unit cell	a= 4.9920 Å c= 17.0690 Å
I/Ic	3.59
Calc. density	2.707 g/cm³
Reference	Sitepu H., O´Connor B H, Li D., "Comparative evaluation of the March and generalized spherical harmonicpreferred orientation models using X-ray diffraction data for molybditeand calcite powdersNote: GSH modelLocality: synthetic", Journal of Applied Crystallography **38**, 158-167 (2005)

Candidates

Name	***Formula***	***Entry No.***	***FoM***
(Os0.2 V0.8)	Os0.2 V0.8	96-152-2775	0.8137
(Ga0.4 Re0.6)	Ga0.4 Re0.6	96-152-2718	0.7979
(Fe0.9 Ni0.1)	Fe0.9 Ni0.1	96-152-2985	0.7911
	Ga Rh	96-154-0931	0.7591
Co2 (Cr0.2 Mn0.8) Ga	Co2 Cr0.2 Ga Mn0.8	96-152-5318	0.7553
	Co O2	96-152-2028	0.7517
(Co2 Ni3) (Er0.5 Sm0.5)	Co2 Er0.5 Ni3 Sm0.5	96-152-5020	0.7491
(Ti V99)0.02	Ti0.02 V1.98	96-154-0339	0.7486
(Cr0.5 Mo0.5)	Cr0.5 Mo0.5	96-152-4009	0.7475
	Co2 Mn Sn	96-152-5317	0.7455
(Co3 Ni2) Er	Co3 Er Ni2	96-152-4273	0.7441
(Tc0.8 Si0.2)	Si0.2 Tc0.8	96-152-7279	0.7360
	Ga Ir	96-152-3838	0.7343
Mg B2	B2 Mg	96-152-6508	0.7275

Ni2 B	B Ni2	96-151-1266	0.7262
(Co0.5 Ni.5) Ti	Co0.5 Ni0.5 Ti	96-152-4742	0.7173
(Ru0.8 V0.2)	Ru0.8 V0.2	96-152-7977	0.7169
	Ru Ta	96-153-8192	0.7159
(Ir0.18 V0.82)	Ir0.18 V0.82	96-152-3685	0.7049
(Ni0.77 Ta0.23)	Ni0.77 Ta0.23	96-152-2811	0.7043
	Ga Ru	96-152-3921	0.7036
	Co2 Mn Sn	96-152-5369	0.7015
	Mn Ni2 Sb	96-153-9555	0.7007
	Dy Ga3	96-152-4227	0.7000
	Ga2 Sc	96-152-2721	0.6990
	Ni2 Si	96-152-3552	0.6973
(Mo W)	Mo W	96-152-3321	0.6956
(Re0.2 W0.8)	Re0.2 W0.8	96-152-3317	0.6951
(Mo Pt)	Mo Pt	96-152-3628	0.6948
	Co2 Sn V	96-152-4755	0.6940
	Mn Ni2 Sb	96-153-8223	0.6932
(Fe0.08 Ti0.092 V0.828)	Fe0.08 Ti0.092 V0.828	96-152-2405	0.6925
(Cu0.255 Zn0.745)	Cu0.255 Zn0.745	96-152-5235	0.6925
Copper(I) oxide (Cuprite)	Cu2 O	96-100-0064	0.6869
Copper(I) oxide (Cuprite)	Cu2 O	96-101-0927	0.6869
	Cd Li3	96-152-5522	0.6857
V D0.77	D0.77 V	96-153-3680	0.6853
(Ti V)	Ti V	96-152-7472	0.6840
	Mn Pd	96-152-2754	0.6832
	Pd	96-151-2532	0.6818
(Al0.94 Co0.06)3 Ti	Al2.82 Co0.18 Ti	96-152-2935	0.6812
(Mo2 Ti)0.66	Mo1.334 Ti0.666	96-153-7811	0.6798
(Mo0.576 Pt0.424)	Mo0.576 Pt0.424	96-152-3722	0.6746
(Cu0.85 Ge0.15)	Cu0.85 Ge0.15	96-152-4232	0.6746
(Hf0.1 Pt0.9)	Hf0.1 Pt0.9	96-152-2516	0.6740
	Re	96-153-4940	0.6732
(Os0.1 W0.9)	Os0.1 W0.9	96-152-2992	0.6731
(Ru0.15 W0.85)	Ru0.15 W0.85	96-152-7974	0.6724
(Pt9 Sn)0.4	Pt3.6 Sn0.4	96-153-9191	0.6722
Copper(I) oxide (Cuprite)	Cu2 O	96-101-0964	0.6713
(Nb0.19 Ni0.81)	Nb0.19 Ni0.81	96-152-2809	0.6712
La Rh3 B	B La Rh3	96-151-1211	0.6708
and 115 others...			

Search-Match

Settings	
Reference database used	COD-Inorg REV214414 2019.03.29
Automatic zeropoint adaptation	Yes
Minimum figure-of-merit (FoM)	0.60
Parameterinfluence 2theta	0.50
Parameterinfluence intensities	0.50
Parameter multiple/single phase(s)	0.50

Peak List

No.	*2theta [°]*	*d [Å]*	*I/I0*	*FWHM*	*Matched*
1	20.88	4.2514	202.13	0.2000	A
2	22.12	4.0148	80.07	0.2000	
3	26.68	3.3380	1000.00	0.2000	A
4	29.48	3.0277	114.12	0.2000	B
5	36.58	2.4542	132.78	0.2000	A
6	39.52	2.2787	119.83	0.2000	A,B
7	40.33	2.2346	96.34	0.2000	A
8	42.50	2.1252	107.29	0.4000	A
9	45.85	1.9773	97.78	0.2000	A
10	47.50	1.9127	82.02	0.2000	B
11	48.62	1.8711	85.90	0.4000	B
12	50.18	1.8166	123.79	0.2000	A
13	54.81	1.6736	100.75	0.2000	A
14	57.41	1.6038	82.51	0.4000	A,B
15	60.04	1.5396	138.97	0.4000	A
16	64.09	1.4518	83.91	0.2000	A
17	68.13	1.3752	136.81	0.2000	A
18	73.58	1.2863	104.79	0.2000	A,B
19	75.74	1.2548	88.29	0.2000	A
20	77.76	1.2272	85.98	0.4000	A

Integrated Profile Areas

Based on calculated profile

Profile area	***Counts***	***Amount***

Overall diffraction profile	31334	100.00%
Background radiation	6527	20.83%
Diffraction peaks	24806	79.17%
Peak area belonging to selected phases	19812	63.23%
Peak area of phase A (Silicon oxide Quartz low)	*18922*	*60.39%*
Peak area of phase B (Calcite)	*890*	*2.84%*
Unidentified peak area	4994	15.94%

Peak Residuals

Peak data	*Counts*	*Amount*
Overall peak intensity	4878	100.00%
Peak intensity belonging to selected phases	4397	90.14%
Unidentified peak intensity	481	9.86%

Diffraction Pattern Graphics

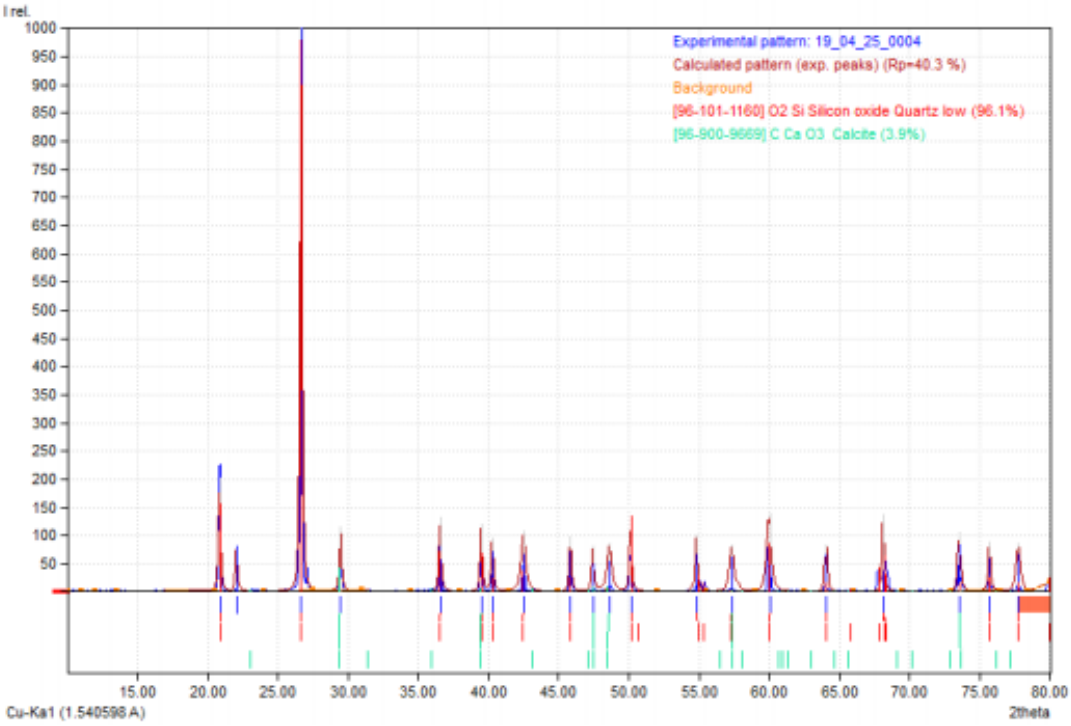

B

S2 Match report

Match! Phase Analysis Report

Sample: 19_04_25_0005

Sample Data

File name	19_04_25_0005.xye
File path	C:/Users/2fik-pc/Desktop/Important/المذكرة/xr
Data collected	May 30, 2019 00:51:50
Data range	10.000° - 80.000°
Original data range	10.000° - 80.000°
Number of points	701
Step size	0.100
Rietveld refinement converged	No
Alpha2 subtracted	No
Background subtr.	No
Data smoothed	No
Radiation	X-rays
Wavelength	1.540598 Å

Matched Phases

Index	*Amount (%)*	*Name*	*Formula sum*
A	88.6	Silicon oxide $-alpha Quartz low	O2 Si
B	6.6	Calcite	C Ca O3
C	4.9	Tellurium	Te
	73.2	*Unidentified peak area*	

A: Silicon oxide $-alpha Quartz low (88.6 %)

Formula sum	O2 Si
Entry number	96-101-1173
Figure-of-Merit (FoM)	0.951534
Total number of peaks	35
Peaks in range	21
Peaks matched	18
Intensity scale factor	0.15
Space group	P 31 2 1
Crystal system	trigonal (hexagonal axes)
Unit cell	a= 4.9130 Å c= 5.4050 Å
I/Ic	3.28
Meas. density	2.660 g/cm³
Calc. density	2.649 g/cm³
Reference	Brill R, Hermann C, Peters C, "Studien ueber chemische Bindung mittels Fourieranalyse III. Die Bindungim Quarz", Naturwissenschaften **27**, 676-677 (1939)

B: Calcite (6.6 %)

Formula sum	C Ca O3
Entry number	96-901-6707
Figure-of-Merit (FoM)	0.764869
Total number of peaks	43
Peaks in range	24
Peaks matched	5
Intensity scale factor	0.01
Space group	R -3 c
Crystal system	trigonal (hexagonal axes)
Unit cell	a= 4.9844 Å c= 17.0376 Å
I/Ic	3.11
Calc. density	2.720 g/cm³
Reference	Ondrus P., Veselovsky F., Gabasova A., Hlousek J., Srein V., Vavrnn I., Skala R., Sejkora J., Drabek M., "Primary minerals of the Jachymov ore district", Journal of the Czech Geological Society **48**, 19-147 (2003)

C: Tellurium (4.9 %)

Formula sum	Te
Entry number	96-101-1099
Figure-of-Merit (FoM)	0.721655
Total number of peaks	33
Peaks in range	20
Peaks matched	5
Intensity scale factor	0.04
Space group	P 31 2 1
Crystal system	trigonal (hexagonal axes)
Unit cell	a= 4.4540 Å c= 5.9240 Å
I/Ic	16.25
Meas. density	6.310 g/cm³
Calc. density	6.245 g/cm³
Reference	Bradley A J, "The crystal structure of tellurium", Philosophical Magazine, Serie 6 (1901-1925) **48**, 477-496 (1924)

Candidates

Name	Formula	Entry No.	FoM
	O2 Si	96-710-3015	0.9517
Silicon oxide $-alpha (Quartz low)	O2 Si	96-101-1173	0.9511
Silicon oxide (Quartz)	O2 Si	96-500-0036	0.9508
Quartz	O2 Si	96-901-3322	0.9504
Quartz	O2 Si	96-900-5018	0.9498
Silicon oxide $-alpha (Quartz low)	O2 Si	96-101-1098	0.9496
Quartz	O2 Si	96-901-2601	0.9467
	O2 Si	96-210-0189	0.9466
Silicon oxide (Quartz low)	O2 Si	96-101-1160	0.9459
Si O2	O2 Si	96-153-8065	0.9411
Quartz	O2 Si	96-900-0776	0.9389
Quartz	O2 Si	96-900-9667	0.9314
Si O2	O2 Si	96-152-6861	0.9231
Quartz	O2 Si	96-901-0146	0.9189
Silicon oxide - $-alpha (Quartz low)	O2 Si	96-101-1177	0.9180
	O2 Si	96-230-0371	0.9177
Si O2	O2 Si	96-153-6390	0.9100
	Be F2	96-153-1932	0.8956
Si O2	O2 Si	96-153-2513	0.8883
Berlinite	Al O4 P	96-900-6550	0.8804
Quartz	O2 Si	96-901-0147	0.8783
Berlinite	Al O4 P	96-900-6551	0.8630
Quartz	O2 Si	96-901-0145	0.8449
Quartz	O2 Si	96-900-5019	0.8358
(Fe0.9 Ni0.1)	Fe0.9 Ni0.1	96-152-2985	0.8148
Quartz	O2 Si	96-901-1494	0.8039
	Ba6 Nb3 O13.5	96-400-1053	0.7863
N2 H4 H2 O	H6 N2 O	96-231-0627	0.7804
Sr Ga Sn	Ga Sn Sr	96-153-9880	0.7791
	O7 P2 Si	96-591-0161	0.7775
Li S H	H Li S	96-153-2759	0.7767
	B N	96-900-8998	0.7743
hexagonal boron nitride	B N	96-201-6171	0.7740
Quartz	O2 Si	96-901-5023	0.7714
	Mo	96-400-1314	0.7679
	Fe Ga12 Ho4	96-431-4515	0.7668
(Mo0.95 Pd0.05)	Mo0.95 Pd0.05	96-152-3804	0.7640
(Mo65 Rh35)0.02	Mo1.3 Rh0.7	96-153-8255	0.7629
(Nb0.125 Ni0.75 Ti0.125)	Nb0.125 Ni0.75 Ti0.125	96-152-2733	0.7622
	O8 Pb Se2 U	96-431-7668	0.7612
Calcite	C Ca O3	96-901-6707	0.7607
	Mo	96-400-1309	0.7600
CaCO3	C Ca O3	96-702-0140	0.7572
	Rh Sm	96-231-0184	0.7519
Ba3 (Nb2 O8)	Ba3 Nb2 O8	96-153-2153	0.7516
Yttrium iodide	I3 Y	96-220-6575	0.7515
Molybdenum	Mo	96-900-8544	0.7512
(Mo0.984 Ni0.016)	Mo0.984 Ni0.016	96-152-3377	0.7487
	Ga2 Sc	96-152-2721	0.7466
	Mn Ni2 Sb	96-153-9555	0.7460
dirubidium heptaoxodimolybdate	Mo2 O7 Rb2	96-201-5446	0.7430
	Ru V	96-152-7981	0.7423

and 150 others...

Search-Match

Settings

Reference database used	COD-Inorg REV214414 2019.03.29
Automatic zeropoint adaptation	Yes
Minimum figure-of-merit (FoM)	0.60
2theta window for peak corr.	0.30 deg.
Minimum rel. int. for peak corr.	1
Parameter/influence 2theta	0.50
Parameter/influence intensities	0.50
Parameter multiple/single phase(s)	0.50

Peak List

No.	2theta [°]	d [Å]	I/I0	FWHM	Matched
1	21.10	4.2070	214.39	0.2000	A
2	26.89	3.3130	1000.00	0.2000	A
3	27.71	3.2164	155.46	0.2000	C
4	29.69	3.0068	134.29	0.2000	B
5	36.79	2.4409	116.88	0.2000	A
6	39.72	2.2672	118.23	0.2000	A,B
7	40.55	2.2229	113.17	0.2000	A,C
8	42.72	2.1147	136.82	0.2000	A
9	46.03	1.9703	105.37	0.2000	A,C

10	48.80	1.8646	98.15	0.4000	B
11	50.40	1.8090	129.78	0.4000	A
12	55.00	1.6682	116.13	0.2000	A
13	60.22	1.5354	146.01	0.2000	A
14	64.28	1.4479	98.73	0.2000	A
15	66.00	1.4143	98.99	0.2000	A,B,C
16	68.29	1.3724	134.08	0.2000	A
17	73.70	1.2845	102.08	0.2000	A,B,C
18	75.95	1.2519	103.39	0.2000	A
19	77.93	1.2249	99.48	0.2000	A

Integrated Profile Areas

Based on calculated profile

Profile area	Counts	*Amount*
Overall diffraction profile	35030	100.00%
Background radiation	5708	16.29%
Diffraction peaks	29323	83.71%
Peak area belonging to selected phases	3674	10.49%
Peak area of phase A (Silicon oxide $-alpha Quartz low)	2595	7.41%
Peak area of phase B (Calcite)	249	0.71%
Peak area of phase C (Tellurium)	830	2.37%
Unidentified peak area	25649	73.22%

Peak Residuals

Peak data	Counts	*Amount*
Overall peak intensity	7740	100.00%
Peak intensity belonging to selected phases	6035	77.98%
Unidentified peak intensity	1704	22.02%

Diffraction Pattern Graphics

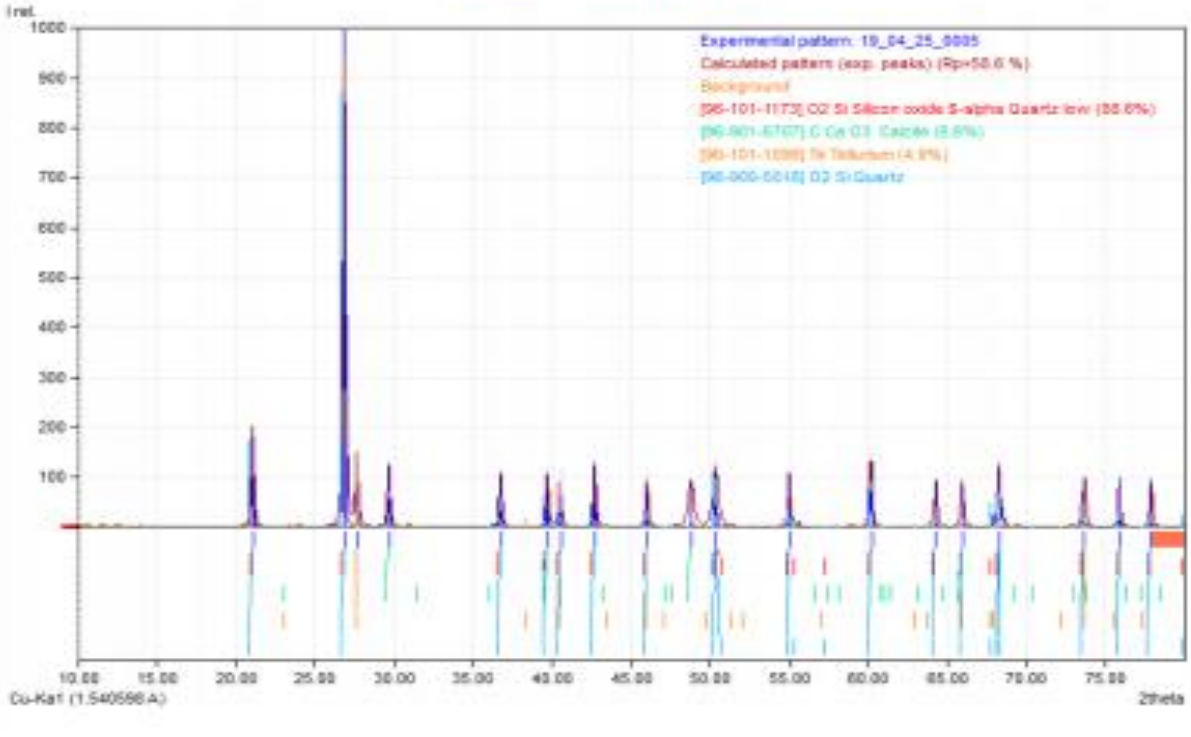

C

S3 Match report

Match! Phase Analysis Report

Sample: 19_04_25_0006

Sample Data

File name	19_04_25_0006.xye
File path	C:/Users/2fik-pc/Desktop/Important/المذكرة/xr
Data collected	May 30, 2019 00:52:01
Data range	10.230° - 80.230°
Original data range	10.000° - 80.000°
Number of points	701
Step size	0.100
Rietveld refinement converged	No
Alpha2 subtracted	No
Background subtr.	No
Data smoothed	No
2theta correction	0.23°
Radiation	X-rays
Wavelength	1.540598 Å

Matched Phases

Index	*Amount (%)*	*Name*	*Formula sum*
A	100.0	Si O2	O2 Si
	46.2	*Unidentified peak area*	

A: Si O2 (100.0 %)

Formula sum	O2 Si
Entry number	96-210-6356
Figure-of-Merit (FoM)	0.815326
Total number of peaks	34
Peaks in range	20
Peaks matched	4
Intensity scale factor	1.00
Space group	P 32 2 1
Crystal system	trigonal (hexagonal axes)
Unit cell	a= 4.7650 Å c= 5.2960 Å
I/Ic	3.08
Calc. density	2.874 g/cm³
Reference	d'Amour H., Denner W., Schulz H., "Structure determination of alpha-quartz up to 68*10exp8 Pa", Acta Crystallographica B (24,1968-38,1982) **35**, 550-555 (1979)

Candidates

Name	*Formula*	*Entry No.*	*FoM*
	Cu Hf2	96-152-4981	0.7856
	Cl K0.4 Na0.6	96-900-3259	0.7688
	Cl K0.4 Na0.6	96-900-3253	0.7687
	Cl K0.4 Na0.6	96-900-3254	0.7687
	Cl K0.4 Na0.6	96-900-3222	0.7679
Tm B2	B2 Tm	96-151-0847	0.7654
silver molybdate	Ag2 Mo O4	96-722-2297	0.7643
Panguite	O3 Ti1.67	96-901-4506	0.7591
(Co0.8 Rh0.2)	Co0.8 Rh0.2	96-152-4725	0.7553
Ta6 Br14	Br14 Ta6	96-810-3874	0.7520
Lu B2	B2 Lu	96-151-0750	0.7494
	Ga3 Pt5	96-152-3254	0.7493
Y6 Ni14.92 P10.18	Ni14.92 P10.18 Y6	96-153-3769	0.7487
(Lu0.95 V0.05) B2	B2 Lu0.95 V0.05	96-151-0749	0.7485
Montetrisaite	Cu3 H7.3 O8 S0.5	96-901-3783	0.7483
Yb B2	B2 Yb	96-151-0856	0.7450
Zr6 Cl14 C	C Cl14 Zr6	96-153-1028	0.7416
	C13 H36 Si4	96-600-0197	0.7409
	Al2 Ca2 O7 Si	96-412-4700	0.7370
(Ca0.5 Sr0.5) Si2	Ca0.5 Si2 Sr0.5	96-153-5999	0.7367
	Mn Pd3	96-152-3903	0.7347
	Pd Zn2	96-152-3177	0.7336
	Br Tl	96-900-8826	0.7320
	Pt8 Ti	96-152-2697	0.7311
Iron trifluoride	F3 Fe	96-100-0477	0.7306
(Mo0.25 Pd0.25 Rh0.25 Ru0.25)	Mo0.25 Pd0.25 Rh0.25 Ru0.25	96-152-2625	0.7305
Cohenite	C Fe3	96-901-6183	0.7302
Selenium	Se	96-901-1652	0.7300
Sr (Sn0.5 Fe0.5) O3	Fe0.5 O3 Sn0.5 Sr	96-153-3398	0.7290
	Cu2 Ni Sn	96-152-5228	0.7284
	Al Ca Si	96-210-0611	0.7284
Neodymium chromium oxyarsenide (NdCrAsO)	As Cr Nd O	96-433-6805	0.7283
	Cu Ni5 Sn9 Zn5	96-200-9420	0.7279

	Mo1.45 Re0.55	96-153-8774	0.7270
(Mo0.31 Ru0.69)	Mo0.31 Ru0.69	96-152-2758	0.7269
Ba8 Fe1.332 Sc4 U2.668 O24	Ba8 Fe1.332 O24 Sc4 U2.668	96-154-1332	0.7266
(Mo0.85 Rh0.15)	Mo0.85 Rh0.15	96-152-3805	0.7251
Potassium scandium sulfide	K S2 Sc	96-202-0008	0.7250
	Ru0.8 Ta1.2	96-153-9012	0.7248
	Ag I	96-901-1697	0.7242
(Mn25 Pd75)0.04	Mn Pd3	96-153-7677	0.7240
Europium silver silicon (1/0.6771.33)	Ag0.67 Eu Si1.33	96-150-9021	0.7238
Grey selenium	Se	96-722-8525	0.7238
	Al Ca Si	96-210-0610	0.7233
(Nb9 Pd41)0.08	Nb0.72 Pd3.28	96-153-8100	0.7228
	Ag As Se2	96-150-9201	0.7216
Ca Y Al3 O7	Al3 Ca O7 Y	96-153-7168	0.7215
	Nb5 Ni	96-152-2277	0.7214
Ti Br2	Br2 Ti	96-153-5972	0.7212
Ru4 Zn12	Ru Zn3	96-700-7707	0.7210
Palladium	Pd	96-900-8479	0.7199
	Ir3 Mo	96-152-3681	0.7198

and 150 others...

Search-Match

Settings

Reference database used	COD-Inorg REV214414 2019.03.29
Automatic zeropoint adaptation	Yes
Minimum figure-of-merit (FoM)	0.60
2theta window for peak corr.	0.30 deg.
Minimum rel. int. for peak corr.	1
Parameter/influence 2theta	0.50
Parameter/influence intensities	0.50
Parameter multiple/single phase(s)	0.50

Peak List

No.	*2theta [°]*	*d [Å]*	*I/I0*	*FWHM*	*Matched*
1	12.23	7.2313	93.89	0.4000	
2	21.48	4.1344	231.41	0.2000	A
3	23.85	3.7280	87.23	0.4000	
4	27.29	3.2650	1000.00	0.2000	A
5	30.07	2.9692	137.57	0.2000	
6	31.76	2.8150	86.82	0.6000	
7	37.22	2.4138	133.22	0.2000	
8	40.13	2.2454	115.90	0.4000	
9	40.96	2.2016	90.26	0.4000	
10	43.09	2.0978	114.60	0.2000	
11	43.90	2.0609	88.46	0.4000	A
12	46.47	1.9526	106.36	0.2000	
13	48.22	1.8858	88.85	0.4000	
14	49.18	1.8512	89.27	0.4000	
15	50.80	1.7959	149.87	0.2000	
16	55.59	1.6519	102.72	0.4000	
17	60.63	1.5260	171.98	0.2000	
18	64.69	1.4398	86.86	0.2000	
19	66.37	1.4073	85.63	0.4000	
20	68.57	1.3674	139.71	0.6000	
21	71.05	1.3256	89.35	0.4000	
22	74.11	1.2784	90.55	0.2000	
23	76.28	1.2473	91.90	0.4000	
24	78.23	1.2210	93.23	0.4000	A

Integrated Profile Areas

Based on calculated profile

Profile area	*Counts*	*Amount*
Overall diffraction profile	17374	100.00%
Background radiation	3724	21.43%
Diffraction peaks	13650	78.57%
Peak area belonging to selected phases	5632	32.42%
Peak area of phase A (Si O2)	*5632*	*32.42%*
Unidentified peak area	8018	46.15%

Peak Residuals

Peak data	*Counts*	*Amount*
Overall peak intensity	3077	100.00%
Peak intensity belonging to selected phases	2501	81.29%
Unidentified peak intensity	576	18.71%

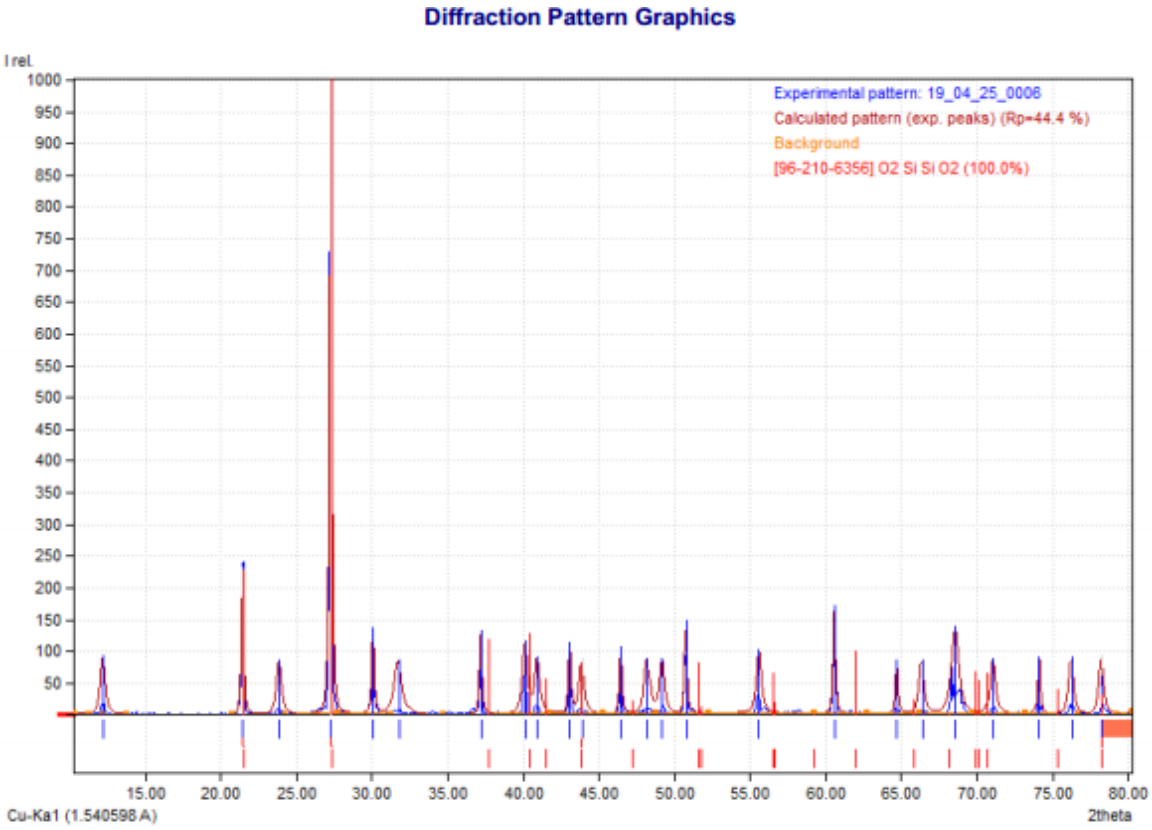
Diffraction Pattern Graphics
I rel.
Experimental pattern: 19_04_25_0006
Calculated pattern (exp. peaks) (Rp=44.4 %)
Background
[96-210-6356] O2 Si Si O2 (100.0%)
Cu-Ka1 (1.540598 A)
2theta

D

S4 Match report

Match! Phase Analysis Report

Sample: 19_04_25_0003

Sample Data

File name	19_04_25_0003.xye
File path	C:/Users/2fik-pc/Desktop/Important/المذكرة/xr
Data collected	May 30, 2019 00:51:30
Data range	19.990° - 79.990°
Original data range	20.000° - 80.000°
Number of points	601
Step size	0.100
Rietveld refinement converged	No
Alpha2 subtracted	No
Background subtr.	No
Data smoothed	No
2theta correction	-0.01°
Radiation	X-rays
Wavelength	1.540598 Å

Matched Phases

Index	*Amount (%)*	*Name*	*Formula sum*
A	94.4	Silicon oxide Quartz low	O2 Si
B	5.6		C Ca O3
	19.3	*Unidentified peak area*	

A: Silicon oxide Quartz low (94.4 %)

Formula sum	O2 Si
Entry number	96-101-1160
Figure-of-Merit (FoM)	0.957609
Total number of peaks	35
Peaks in range	35
Peaks matched	12
Intensity scale factor	0.78
Space group	P 32 2 1 S
Crystal system	trigonal (hexagonal axes)
Unit cell	a= 4.9100 Å c= 5.4000 Å
I/Ic	3.37
Meas. density	2.660 g/cm³
Calc. density	2.654 g/cm³
Reference	Machatschki F, "Kristallstruktur von Tiefquarz", Fortschritte der Mineralogie **20**, 45-47 (1936)

B: C Ca O3 (5.6 %)

Formula sum	C Ca O3
Entry number	96-450-2444
Figure-of-Merit (FoM)	0.752433
Total number of peaks	43
Peaks in range	43
Peaks matched	2
Intensity scale factor	0.05
Space group	R -3 c
Crystal system	trigonal (hexagonal axes)
Unit cell	a= 4.9758 Å c= 16.9921 Å
I/Ic	3.45
Calc. density	2.737 g/cm³
Reference	Zolotoyabko E., Caspi E. N., Fieramosca J. S., Von Dreele R. B., Marin F., Mor G., Addadi L., Weiner S., Politi Y., "Differences between Bond Lengths in Biogenic and Geological Calcite", Design' **10(3)**, 1207 (2010)

Candidates

Name	*Formula*	*Entry No.*	*FoM*
Ni2 B	B Ni2	96-151-1266	0.7786
Helium	He	96-901-1637	0.7118
	Co O2	96-152-2028	0.6801
Algodonite	As0.1 Cu0.9	96-901-5529	0.6795
(Al0.94 Co0.06)3 Ti	Al2.82 Co0.18 Ti	96-152-2935	0.6757
Copper(I) oxide (Cuprite)	Cu2 O	96-100-0064	0.6730
Copper(I) oxide (Cuprite)	Cu2 O	96-101-0927	0.6730
(Pd0.5 Rh0.5)3 Zr	Pd1.5 Rh1.5 Zr	96-152-2724	0.6724
	Ga3 Ho Mn0.152	96-400-1867	0.6722
Periclase	Mg O	96-901-3230	0.6705
Mg B2	B2 Mg	96-152-6508	0.6702
(Ni0.77 Ta0.23)	Ni0.77 Ta0.23	96-152-2811	0.6690
	C4 Fe Sc3	96-410-9721	0.6673
(Cu0.85 Ge0.15)	Cu0.85 Ge0.15	96-152-4232	0.6642
	Nb Ni3	96-153-7950	0.6632

Iron germanium (3:1)	Fe3 Ge	96-100-1145	0.6629
	Ga2 Sc	96-152-2721	0.6626
Algodonite	As0.111 Cu0.889	96-901-4014	0.6605
	Ga3 U	96-152-3640	0.6594
	Be F2	96-153-1932	0.6559
Periclase	Mg O	96-900-6460	0.6550
(Li0.275 Ni0.725) O	Li0.275 Ni0.725 O	96-400-2257	0.6549
Periclase	Mg O	96-901-3206	0.6540
Periclase	Mg O	96-900-0497	0.6526
Periclase	Mg O	96-900-6755	0.6526
(Nb0.19 Ni0.81)	Nb0.19 Ni0.81	96-152-2809	0.6507
Cerium palladium antimonide (8/24/1)	Ce8 Pd24 Sb	96-100-5034	0.6498
	Ca2 Ir12 P7	96-153-6713	0.6453
	Nb Ni3	96-152-2734	0.6404
Mn2 Pd6 D	D Mn2 Pd6	96-154-1175	0.6398
Nickel boride (2/1)	B Ni2	96-101-0477	0.6372
(Pd0.845 Zr0.155)	Pd0.845 Zr0.155	96-152-2600	0.6371
Yixunite	In0.5 Pt0.5	96-900-9697	0.6345
Periclase	Mg O	96-900-6754	0.6337
	Fe Ga12 Ho4	96-431-4515	0.6331
	Er4 Fe0.67 Ga12	96-431-4517	0.6329
	Ce Ga3 Pd2	96-152-7130	0.6322
(In Pt9)0.4	In0.4 Pt3.6	96-153-9194	0.6281
(Pt9 Sn)0.4	Pt3.6 Sn0.4	96-153-9191	0.6270
(Ce0.05 Ru0.95)	Ce0.05 Ru0.95	96-152-5250	0.6259
	Er4 Fe Ga12	96-431-4516	0.6255
	Ir3 Zr	96-153-7869	0.6251
(Hf0.1 Pt0.9)	Hf0.1 Pt0.9	96-152-2516	0.6243
	Re	96-153-4940	0.6234
La Rh3 B	B La Rh3	96-151-1212	0.6224
praseodymium manganese copper phosphide (2/3/9/7)	Cu9 Mn3 P7 Pr2	96-433-3628	0.6215
	Pd	96-151-2532	0.6211
neodymium manganese copper phosphide (2/3/9/7)	Cu9 Mn3 Nd2 P7	96-433-3629	0.6206
	Dy4 Fe Ga12	96-431-4514	0.6203
	Ga3 Ho Mn0.08	96-400-1866	0.6201
Sm Pt5 Si3	Pt5 Si3 Sm	96-810-4444	0.6188
Periclase	Mg O	96-901-3258	0.6173
and 17 others...			

Search-Match

Settings

Reference database used	COD-Inorg REV214414 2019.03.29
Automatic zeropoint adaptation	Yes
Minimum figure-of-merit (FoM)	0.60
2theta window for peak corr.	0.30 deg.
Minimum rel. int. for peak corr.	1
Parameter/influence 2theta	0.50
Parameter/influence intensities	0.50
Parameter multiple/single phase(s)	0.50

Peak List

No.	*2theta [°]*	*d [Å]*	*I/I0*	*FWHM*	*Matched*
1	20.90	4.2474	183.14	0.2000	A
2	26.71	3.3344	1000.00	0.2000	A
3	29.51	3.0248	139.69	0.2000	B
4	36.63	2.4515	129.92	0.2000	A
5	39.54	2.2775	113.22	0.2000	A,B
6	42.52	2.1244	116.91	0.2000	A
7	45.90	1.9757	114.83	0.4000	A
8	50.23	1.8149	131.88	0.2000	A
9	55.02	1.6677	120.58	0.2000	A
10	60.06	1.5393	114.43	0.2000	A
11	64.13	1.4510	108.04	0.2000	A
12	68.06	1.3765	132.69	0.2000	A

Integrated Profile Areas

Based on calculated profile

Profile area	*Counts*	*Amount*
Overall diffraction profile	42812	100.00%
Background radiation	7734	18.06%
Diffraction peaks	35078	81.94%
Peak area belonging to selected phases	26833	62.68%
Peak area of phase A (Silicon oxide Quartz low)	*25037*	*58.48%*
Peak area of phase B (C Ca O3)	*1796*	*4.19%*
Unidentified peak area	8246	19.26%

Peak data	*Counts*	*Amount*
Overall peak intensity	7877	100.00%
Peak intensity belonging to selected phases	7400	93.95%
Unidentified peak intensity	476	6.05%

Diffraction Pattern Graphics

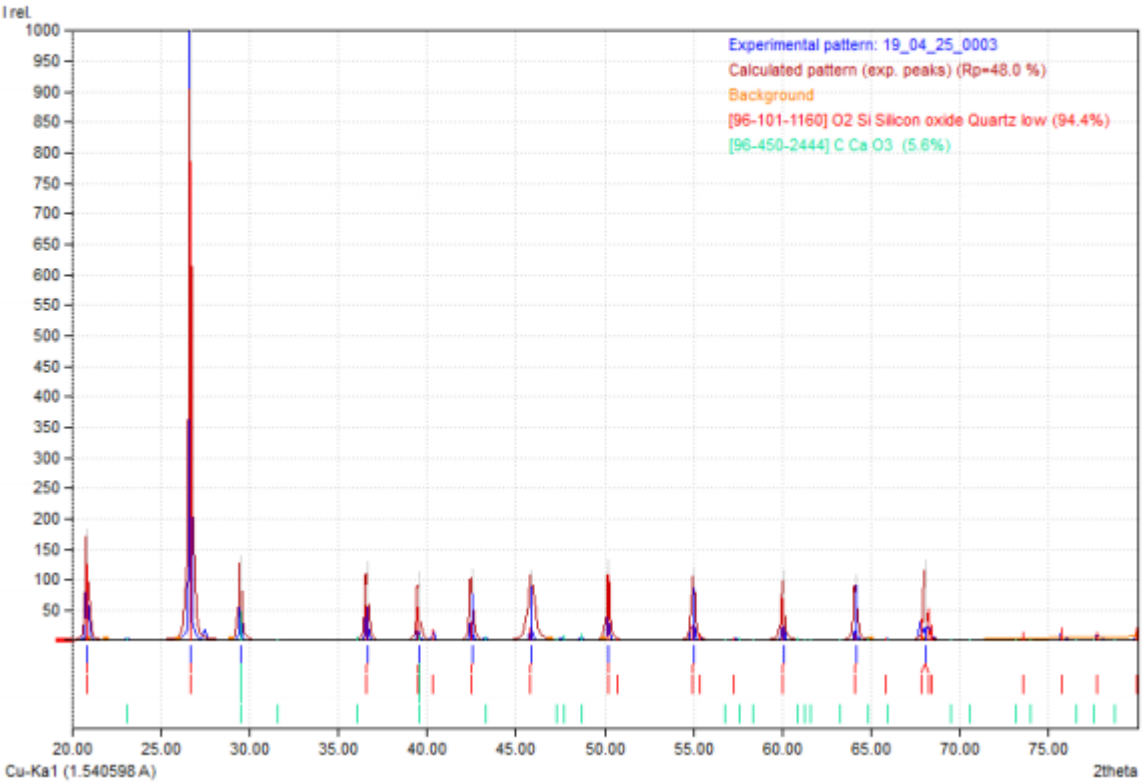

Bibliography

[1] Mehdadi Nouia, " composition determination of sand color genera of Ourgla dunes", Doctorate thesis", University of Ouragla, P.2-5, 20,37,38, (2017)

[2] Kok J F, Parteli E J R, Michaels T I and Bou Karam ,The physics of windblown sand and dust, Rep. Prog. Phys. 75 106901, (2012)

[3] Ralph D. Lorenz James R. Zimbelman, How Windblown Sand Shapes Planetary Landscapes, Springer, Berlin Heidelberg, p 17-23,(2014).

[4] www.universetoday.com/139502/theres-sand-on-titan-where-does-it-come-from-1/

[5] Kenneth Pye · Haim Tsoar, Aeolian Sand and Sand Dunes, Springer, Berlin Heidelberg, p 142, (2009).

[6] Hakon Wadell, Volume, Shape, and Roundness of Quartz Particles, The Journal of Geology, Vol. 43, No. 3 (1935).

[7] Friedman, G.M., Sanders, J.E, and Kopaska-Merkel, D.C., 1992, Principles of Sedimentary Deposits: Stratigraphy and Sedimentology: Macmillan Publishing Company, New York, 717p.

[8] www.sand.org/page/industrial_sand

[9] Industrial Silica sand, Mining in Minnesota, Minnesota Department of Natural Resources,2012

[10] https://www.ima-na.org/page/what_is_ind_sand

[11] Hans-Rudolf Wenk and Andrei Bulakh, Minerals- Their Constitution and Origin, the University Press, Cambridge, P.313-319,P.117-127,(2004).

[12] A.J. EASTON, Chemical Analysis of Silicate Rocks, Volume 6 - 1st Edition - Elsevier

[13] Samiha Beddiaf, Smail Chihi and Youcef Leghrieb, The determination of some crystallographic parameters of quartz, in the sand dunes of Ouargla, Algeria, Journal of African Earth Sciences, 106, (2015)

[14] Andrew J Barker,A key for identification of rock-forming minerals in thin-section,Balkema Book,P.18-112,(2014)

[15] www.quartzpage.de/gen_struct.html

[16] C. LU, ELSEVIER SCIENCE PUBLISHERS B.V, Amsterdam, The Netherlands, (1984)

[17] www.explainthatstuff.com/piezoelectricity.html

[18] Brian C.Smith, fundamentals of Fourier transform infrared spectroscopy, CRC Press, the United States of America, P.4-11,(2011).

[19] BEDDIAF Samiha, Determination of the molecular composition and the quartz concentration in the different granular types of Ouargla dunes sand using spectroscopic techniques, Doctorate LMD thesis, University of Kasdi Merbah Ouargla, Algeria, P.1-3,(2016).

[20] Kazuo Nakamoto,Infrared and Raman Spectra of Inorganic and Coordination Compounds, Part B: Applications in Coordination, Organometallic, and Bioinorganic Chemistry,Wily,P.45-59,(1997)

[21] www.intechopen.com/books/infrared-spectroscopy-principles-advances-and applications/introductory-chapter-infrared-spectroscopy-a-synopsis-of-the-fundamentals-and-applications

[22] C. Hammond,The Basics of Crystallography and Diffraction,Oxford University Press,University of leeds,P.144-178 ,(2009)

[23] Nassima Meftah and Mohammed Sadok Mahboub, Spectroscopic Characterizations of Sand Dunes Minerals of El-Oued (Northeast Algerian Sahara) by FTIR, XRF and XRD Analyses, Silicon, ISSN 1876-990X, (2019).